Received: 24 June 2025 | Revised: 16 January 2026 | Accepted: 22 January 2026

DOI: 10.1002/alz.71348

Alzheimer's & Dementia®
THE JOURNAL OF THE ALZHEIMER'S ASSOCIATION

RESEARCH ARTICLE

Native PLGA nanoparticles attenuate disease pathology via multiple pathways in 5xFAD Alzheimer's model

Govindarajan Karthivashan[1] | **Shuai Wang**[2] | **Qi Wu**[1] | **Abhishek Dahal**[1] | **Xiuju Li**[1] | **Danny Galleguillos**[3] | **Simonetta Sipione**[3] | **Gopal Thinakaran**[2] | **Satyabrata Kar**[1]

[1]Department of Medicine (Neurology), Centre for Prions and Protein Folding Diseases, University of Alberta, Edmonton, Alberta, Canada

[2]Department of Molecular Medicine, Morsani College of Medicine, Byrd Alzheimer's Center and Research Institute, University of South Florida, Tampa, Florida, USA

[3]Department of Pharmacology, University of Alberta, Edmonton, Alberta, Canada

Correspondence
Satyabrata Kar, Ph.D, Centre for Prions and Protein Folding Diseases, Departments of Medicine (Neurology) and Psychiatry, University of Alberta, Edmonton, Alberta, Canada.
Email: skar@ualberta.ca

Funding information
CIHR, Grant/Award Numbers: MOP-84480, PJT-175090; Alzheimer Society of Alberta and Northwest Territories; National Institute on Aging, National Institutes of Health, Grant/Award Numbers: RF1AG077610, RF1AG079141; Ballermann Translational Research Fellowship; SynAD postdoctoral fellowships

Abstract

INTRODUCTION: Elevated amyloid beta (Aβ) levels and aggregation contribute to neurotoxicity and development of Alzheimer's disease (AD), the leading cause of dementia in the elderly. While we reported that native poly(D,L-lactic-co-glycolic acid) (PLGA) nanoparticles, clinically used in drug delivery, suppress Aβ aggregation/toxicity, their effects in adult 5xFAD mice with advanced Aβ pathology remain unknown.

METHODS: We evaluated the effects of native PLGA in 8-month-old male 5xFAD mice via chronic intracerebroventricular (ICV) infusion using mini osmotic pumps. Cognitive function, amyloid level/burden, synaptic integrity, and neurodegenerative events were assessed along with transcript levels in brain tissues using bulk RNA sequencing (RNA-seq).

RESULTS: PLGA treatment reversed cognitive deficits, reduced Aβ levels/deposits, and attenuated neurodegenerative events. These effects were associated with modulation of Aβ production, oxidative stress, and lysosomal Aβ clearance. RNA-seq revealed transcriptional changes related to vesicle trafficking, immune activity, and redox regulation.

DISCUSSION: Native PLGA, by targeting different facets of the Aβ axis, offer unique therapeutic potential in treating AD-related pathology.

KEYWORDS
5xFAD mice, Alzheimer's disease, amyloid beta, cognitive deficits, nanoparticles, neuroprotection

Highlights

- Elevated Aβ levels/aggregation trigger degeneration of neurons and the development of AD, the most common cause of dementia affecting elderly populations.
- At present there is no effective treatment for AD.

Govindarajan Karthivashan and Shuai Wang have contributed equally to this work.

- Native PLGA nanoparticles, which constitute a family of FDA-approved nanocarriers in delivering drugs in humans, have been shown to prevent Aβ aggregation and toxicity.
- Chronic administration of native PLGA attenuates cognitive deficits and AD-related Aβ pathology in a 5xFAD mouse model of AD.
- Native PLGA nanoparticles without conjugation with any drug/agent exhibit therapeutic potential in the treatment of AD pathology.

1 | BACKGROUND

Alzheimer's disease (AD), the most common neurodegenerative disorder accounting for ~60% of all dementia cases, is characterized neuropathologically by the presence of extracellular neuritic plaques, intracellular neurofibrillary tangles, and the loss of synapses/neurons in selected brain regions. The severely affected regions in AD brains include the hippocampus, neocortex, and some subcortical nuclei. The majority of AD cases are sporadic, whereas only a minority (<10%) of cases segregate with mutations in three known genes: amyloid precursor protein (*APP*), presenilin 1 (*PSEN1*), and *PSEN2*.[1,2] Neuritic plaques consist of extracellular deposition of amyloid beta (Aβ) peptides derived from APP. Full-length APP undergoes proteolytic cleavage through the non-amyloidogenic α-secretase or amyloidogenic β-secretase pathway. The α-secretase processing by a family of disintegrin/metalloproteinase domain-containing proteins (e.g., ADAM10), which occurs primarily in secretory pathways, cleaves APP within the Aβ domain, generating soluble APPα (sAPPα) and a C-terminal fragment (α-CTF). Conversely, the β-secretase cleavage, which occurs mostly in endo-lysosomal organelles, is mediated by the β-site APP cleaving enzyme (BACE1), resulting in the production of sAPPβ and β-CTF. The γ-secretase is a tetrameric complex comprising the presenilin 1 or 2 (PS1/PS2), nicastrin, presenilin enhancer 2 (PEN2), and anterior pharynx defective 1 (APH1).[3,4] The γ-secretase processing of β-CTF and α-CTF generates full-length A$\beta_{1\text{-}40}$/A$\beta_{1\text{-}42}$ or A$\beta_{17\text{-}40}$/A$\beta_{17\text{-}42}$ peptides, respectively. Although A$\beta_{1\text{-}42}$ constitutes ~10% of the total Aβ produced in the normal brain, it aggregates fast and is more toxic to neurons than A$\beta_{1\text{-}40}$.[4,5] While ADAM10 is located in the plasma membrane, synaptic vesicles, and trans-Golgi network, BACE1 is evident primarily in endosomes and presynaptic vesicles. The γ-secretase complex is present in the endoplasmic reticulum, Golgi apparatus, endo-lysosomal compartments, and, to some extent, in plasma membrane.[6–9] Pathological changes that characterize AD indicate that a disparity between Aβ production and clearance, leading to its increased levels, followed by aggregation, contributes to neurodegeneration/development of AD.[10,11] Thus, regulating Aβ levels and/or preventing its aggregation into toxic fragments is a promising strategy for averting the onset of AD or arresting its progression.

Currently, there is no effective treatment for halting the progression of AD. One of the major challenges in developing an effective treatment for AD is the blood–brain barrier (BBB), which prevents the entry of drugs/agents into the brain.[12,13] In the last decade, nanoparticles, which are <100 nm in diameter with unique physiochemical properties, have been extensively studied to overcome the protective BBB in delivering drugs to the targeted areas. Therapeutic strategies utilizing nanoparticles are in different stages of development which includes targeted delivery of various drugs/agents to sequester/interfere with Aβ aggregation/toxicity. Polymorphic nanoparticles conjugated with curcumin, donepezil, memantine, or selegiline have been shown to inhibit Aβ aggregation/toxicity under in vitro conditions and/or decrease Aβ burden as well as cognitive deficits in animal models of AD.[14–16]

Acidic poly(D,L-lactic-co-glycolic acid) (PLGA) nanoparticles, a family of US Food and Drug Administration (FDA)-approved biodegradable polymers, have long been studied as delivery vehicles for drugs/macromolecules. In fact, PLGA is currently being used to deliver 20 FDA-approved drugs for a variety of conditions.[17,18] PLGA is synthesized from glycolic acid and lactic acid. Different forms/resomers of PLGA can be obtained, depending on the ratio of lactide to glycolide used for polymerization, which are readily hydrolyzed in the body.[19] Recent studies showed that PLGA-encapsulated drugs/agents, including donepezil, curcumin, quercetin, and selegiline, could have beneficial effects on cellular/animal models of AD.[20–25] However, very little is known about the implications of native PLGA nanoparticles (i.e., without conjugation with any drug/agent) in physiological conditions and/or disease pathology. Evidence suggests that native PLGA can restore impaired lysosomal function by regulating its pH, implicating a role for PLGA in diseases associated with lysosomal dysfunction.[26,27] Recently, we reported that native PLGA can attenuate Aβ aggregation/toxicity in cellular and animal models of AD.[28–31] In this study, using various experimental approaches, we report that native PLGA may reverse cognitive deficits and attenuate levels of APP/Aβ and amyloid burden in 8-month-old 5xFAD mice by regulating inflammatory response and oxidative stress, thereby revealing its unique, untapped potential in the treatment of AD pathology.

RESEARCH IN CONTEXT

1. **Systematic review**: A comprehensive review of the recent literature on PLGA nanoparticles was conducted using PubMed. Evidence suggests that native PLGA can protect neurons by regulating lysosomal function. Earlier results from our lab also indicated that native PLGA could attenuate Aβ aggregation and toxicity, but its therapeutic effects in adult 5xFAD mouse models of AD displaying cognitive deficits and the full spectrum of Aβ pathology remain unclear.
2. **Interpretation**: Chronic ICV administration of native PLGA using mini osmotic pumps has been shown to reverse both spatial and non-spatial cognitive deficits accompanied by decreased levels/deposits of Aβ peptides and restore synaptic loss and neurodegenerative events. This is mediated by mitigating Aβ production, oxidative stress, and glial responses involving lysosomal Aβ clearance. Our RNA-seq data from mice treated with PLGA revealed marked transcriptional changes, including those that prompt vesicle exocytosis, immune responses, and oxidative stress. These results provide unequivocal evidence that native PLGA nanoparticles, by targeting different facets of amyloid pathophysiology, may offer unique therapeutic potential in treating AD pathology.
3. **Future directions**: Future studies, apart from validating these results, should evaluate the therapeutic efficacy of long-term PLGA treatment. Further work is needed to determine the potential of native PLGA in attenuating tau pathology in an appropriate animal model exhibiting AD-related tau pathology.

2 | METHODS

2.1 | Materials

Dulbecco's modified Eagle's medium, neurobasal medium, Hanks' balanced salt solution, fetal bovine serum, B27, N2 supplement, CultureOne Supplement, Alexa Fluor 488/594 conjugated secondary antibodies, 4% to 12% NuPAGE Bis-Tris gels, ProLong Gold anti-fade reagent, enzyme-linked immunosorbent assay (ELISA) kits for the detection of soluble and insoluble human A$\beta_{1\text{-}40}$ (Catalog No.: KHB3481) and A$\beta_{1\text{-}42}$ (Catalog No.: KHB3441), bicinchoninic acid (BCA) protein assay kit, enhanced chemiluminescence (ECL) kit, and MitoSOX™ Red were purchased from Thermo Fisher Scientific Inc. (Nepean, ON, Canada), while MitoTracker™ Green FM was from Thermo Fisher Scientific (Waltham, MA, USA) and Degradex® PLGA (50:50 resomer; molecular weight 30000; Catalog No.: LG100) was obtained from Phosphorex (Hopkinton, MA, USA). Mouse-specific ELISA kits for the detection of glial fibrillary acidic protein (GFAP; Catalog No.: BSKM61478) and synaptophysin (Catalog No.: BSKM61652) were purchased from Bioss Inc., MA, USA. The ALZET® mini osmotic pumps (Model 2004) and brain infusion kits were procured from DURECT Corp. (Cupertino, CA, USA). The RNeasy mini kit (Catalog No.: 749040) was from Qiagen (Ann Arbor, MI, USA), whereas the cDNA reverse transcription kit (Catalog No.: 4368814), Power SYBR Green Master Mix (Catalog No.: A25742), and QuantStudio3 (Catalog No.: A28567) were from Applied Biosystems (Carlsbad, CA, USA). The Oxyblot™ kit and Fluoro-Jade C were from EMD Millipore (MA, USA). Cellular redox, BACE1 activity, superoxide dismutase (SOD) activity, and DCFDA/H_2DCFDA—Cellular reactive oxygen species (ROS) kits were purchased from Abcam (Cambridge, MA, USA). All horseradish peroxidase-conjugated secondary antibodies were from Bio-Rad (Mississauga, ON, Canada). Sources of primary antibodies used in the study are listed in Table S1. All other chemicals were from either Sigma-Aldrich or Thermo Fisher Scientific.

2.2 | Animals and surgery

The 5xFAD-Tg mice (B6SJL-Tg[APPSwFlLon, PSEN1*M146L*-L286V]6799Vas/Mmjax), which co-overexpress human *APP* and *PSEN1* harboring five familial AD mutations, under the control of the murine Thy1 promoter, were obtained from The Jackson Laboratory (Bar Harbor, ME, USA). To maintain the original hybrid genetic background and consistent transgene expression, hemizygous transgenic males were bred with non-transgenic B6SJLF1/J females. Due to the rapid onset of amyloidosis in females and the known sex differences in amyloid burden in this model,[32] all experiments were conducted using hemizygous 5xFAD male mice and their non-transgenic littermates as wild-type (WT) controls. All the animals were maintained in accordance with Canadian Council on Animal Care guidelines on a 12-h light/dark cycle with access to food and water ad libitum. Eight-month-old 5xFAD and age-matched WT mice underwent stereotaxic surgery to insert a microcannula into the right brain ventricle (−0.8 mm mid/lateral, −0.1 mm antero/posterior and −3.0 mm dorso/ventral from Bregma) under anesthesia. The cannula was connected to a mini osmotic infusion pump (Alzet, Model 2004) implanted subcutaneously on the shoulder of the mouse as described earlier.[29] The pumps were filled and primed to infuse either artificial cerebrospinal fluid (CSF) or native PLGA dissolved in CSF at a flow rate of 0.25 µL/h for 28 days. Considering the volume and rate of synthesis/renewal of the mouse CSF,[33] our treatment conditions should lead to a concentration of 25 µM PLGA in the mouse CSF at equilibrium. All animals were monitored closely over 28 days of treatment for signs of weight loss and abnormal behavior. Following treatment, mice were assigned into four groups (CSF-WT, PLGA-WT, CSF-5xFAD, and PLGA-5xFAD). Randomization was used to allocate transgenic and non-transgenic mice to control and treatment groups. Two independent sets of 12 unique numbers (range: 1 to 30) were generated using a computer-based randomization tool (Research Randomizer) to ensure unbiased group allocation (n = 10 to 12/group caged individually). All animals were subjected to various behavioral tests to assess their cognitive performance prior to decapitation or fixing the brain by perfusion with 4% paraformaldehyde for subsequent analysis. Animals were excluded from the study based on the following predefined criteria:

(i) disconnection of the cannula from the osmotic pump during the treatment period, (ii) dislodgement of the cannula from the surgical site during the treatment period, and (iii) premature death prior to completion of behavioral assessments and/or necropsy.

2.3 | Cognitive tests

To assess cognitive performance, we conducted Morris water maze, Novel Object Recognition, and Y-maze tests in 5xFAD and WT control mice following the intracerebroventricular (ICV) administration of PLGA or CSF for 28 days. The Morris water maze test was carried out to evaluate the spatial reference memory of animals, as described earlier.[34] In brief, all CSF- and PLGA-treated 5xFAD and control mice were given four trials per day (maximum 60 s/trial) for five consecutive days to find a submerged platform in a 2-m-diameter pool of opaque water (24° to 25°C) using distal spatial cues available in the test room. The latency to find the submerged platform is recorded using a computerized tracking system (HVS Image 2100, HVS Image, Buckingham, UK) for both 5xFAD and control mice and then compared to evaluate their cognitive status. On the final day, all animals are given a probe trial (60 s) after removing the submerged platform. The time spent by an animal in the target quadrant and the number of crossings over the missing platform were recorded as a measure of the spatial reference memory and learning capacity. Subsequently, the novel object recognition test was performed in a white acryl plastic chamber to investigate recognition memory, as described earlier.[29] In brief, one day prior to the test, all mice were exposed to the apparatus without objects for 10 min to acclimatize to the environment. On day 1, the animals were allowed to explore freely for 8 min to familiarize themselves with two different objects placed equidistantly from both corners. On the next day, one of the two objects was replaced with a novel object. The exploratory behavior of the mice toward the familiar and novel objects over 8 min was quantified using a memory index, where t_o represents time exploring an object during the original exposure and t_n represents time spent exploring a novel object on re-exposure; memory index = $(t_n - t_o)/(t_n + t_o)$. Finally, the Y-maze test was carried out to assess spatial working memory by allowing the mice to explore unvisited areas/arms of the maze during its subsequent exploration.[35] At the beginning of each trial, the mouse was introduced into the center of the maze, followed by the acquisition of the total number/pattern of arm entries over an 8-min period. The percentage of spontaneous alternations was calculated based on the number of consecutive entries into all three arms, T_{nca}, divided by the number of possible alternations (total arm entries $T_{na} - 2$), that is, the percentage of spontaneous alternations = $T_{nca}/(T_{na} - 2)$.

2.4 | Mouse cortical neuronal cultures and treatments

Primary cortical cultures were prepared from 18-day-old embryos of timed pregnant BALB/c mice (St. Constant, Quebec, Canada) as described earlier.[28,36] In brief, the frontal cortex from pup brains was dissected in Hanks' balanced salt solution supplemented with 10 mM HEPES, 600 μM L-glutamine, 1 mM Na-pyruvate, 30 units/mL penicillin, 30 μg/mL streptomycin, and then digested with TrypLE express. The cell suspension was filtered through a cell strainer and plated on 96-well plates (5×10^4 cells/well) for MitoSOX assay, on eight-well chamber slides (1×10^5 cells/chamber) for MitoSOX imaging, or on six-well plates (2×10^6 cells/well) for biochemical analysis. The cultures were grown at 37°C in a 5% CO_2 humidified atmosphere, and all experiments were performed on day 6 after plating. In brief, cultured neurons were treated with 10 μM A$\beta_{1\text{-}42}$ in the presence or absence of 6 or 25 μM PLGA for 24 h.[28] The control and treated neurons were then processed for various cellular/biochemical assays.

2.5 | RNA isolation and qPCR

Total RNA was isolated from the forebrain tissues of CSF- and PLGA-treated 5xFAD and WT mice ($n = 5$ or 6/group) using the Qiagen RNeasy mini kit. The RNA concentration and integrity were assessed using an Agilent 2100 Bioanalyzer, and samples with an RNA Integrity Number > 9.0 were used for RNA sequencing (RNA-seq) and quantitative reverse transcription polymerase chain reaction (RT-qPCR) analyses. A high-capacity cDNA reverse transcription kit was used for the reverse transcription of 2 μg total RNA in a 20-μL reaction and then 1 μL of 200X diluted cDNA was used for each qPCR reaction. The primer pairs used for qPCR were chosen from the Primer Bank database (see Supplementary-Data File 1) and synthesized by Integrated DNA Technologies (Coralville, IA, USA). qPCRs were performed using 500 nM PCR primers and Power SYBR Green Master Mix on QuantStudio3 with three technical replicates for each biological sample. The qPCR parameters were as follows: 95°C for 3 min, then 40 cycles of 95°C for 15 s and 60°C for 30 s. The $2^{-\Delta\Delta Ct}$ method was used to calculate the relative abundance of transcripts.[37]

2.6 | mRNA RNAseq and data analysis

Paired-ended sequencing was performed on Illumina's NovaSeq 6000 sequencing system (LC Sciences). Sequence adapters and low-quality reads were removed using Cutadapt. Quality control checks on raw sequence data were performed with FastQC. Sequencing reads were then mapped to the mouse reference genome (release-96) using the HISAT program. After the final transcriptome was generated, the R package DESeq2 was used to estimate the expression levels of all transcripts (Supplementary-Data File 1). Differentially expressed genes (DEGs) from different comparisons were identified using the following criteria: fold change (FC) ≥ 1 for upregulated and ≤ −1 for downregulated DEGs with adjusted $p < 0.01$. Principal component analysis (PCA) was performed to determine the variability and repeatability of samples as described earlier.[37] Volcano plots were generated by the R package EnhancedVolcano (1.20.0) to visualize the overall distribution of DEGs. Gene Ontology (GO) analysis of DEGs was performed using the R Package clusterProfiler (version 3.18.1), and the significance level for GO terms was set at $p < 0.05$. Gene set enrichment analysis (GSEA, version 4.2.3) was performed using the RNA-seq data

(Supplementary-Data File 1) against the gene sets described in the Molecular Signatures Database (version 7.5.1, C2 and C5 categories). The R package vissE (version 1.10.0) was used to exploit this gene set–gene set overlap relationship to enable the interpretation of clusters of gene sets and further summarize results. To identify modules of highly correlated genes, WGCNA was performed on RNA-seq data by the WGCNA package in R (version 1.72-5). To identify modules with different expression patterns, a soft threshold power was assigned to create co-expression networks. Finally, 15 modules with the hub genes and their co-expressed genes were obtained.

2.7 | Western blot analysis

Immunoblotting was carried out on brain tissues of CSF- and PLGA-treated 5xFAD and WT mice (three to five mice/group) as well as on neuronal cultures treated with Aβ and PLGA, as described earlier.[28,29] In brief, tissue and culture samples were first homogenized with radioimmuno-precipitation lysis buffer, and proteins were quantified and normalized using a BCA kit. Denatured samples were resolved on 10% polyacrylamide or 4% to 12% NuPAGE Bis-Tris gels, transferred to PVDF membranes, blocked with 5% milk, and incubated overnight at 4°C with various primary antibodies at dilutions listed in Table S1. The membranes were then exposed to appropriate horseradish peroxidase-conjugated secondary antibodies (1:5000), and immunoreactive proteins were detected using an ECL kit. The blots were reprobed with an anti-β-actin antibody and quantified using ImageJ as described earlier.[29]

2.8 | Immunostaining and histological studies

Coronal brain sections (20 µm) prepared from CSF- and PLGA-treated 5xFAD and WT mice (three to five mice/group) were incubated overnight at 4°C with various antibodies (see enclosed Table S1) and then processed for immunofluorescence or glucose-oxidase detection method as described earlier.[28] Some brain sections were co-labeled with microglia marker CD68 antibody and confirmation-dependent anti-fibrillar Aβ (OC) or anti-IBA1 antibodies. In parallel, some brain sections were immunolabeled with anti-IBA1 or anti-Aβ (6E10) antibodies, followed by Thioflavin S (ThS) staining. Additionally, brain sections were incubated with 0.0001% Fluoro-Jade C in 0.1% acetic acid to label degenerating neurons, dendrites, and axons.[38] The stained sections were then visualized and photographed using a Nikon Eclipse 90i fluorescence microscope with a Retiga 2000R Q imaging system (Nikon Instruments Inc.) or Nano-Zoomer digital slide scanner.

2.9 | BACE1 activity assays

The frontal cortex and hippocampus of 5xFAD and WT control mice (four or five mice/group) treated with CSF or PLGA were processed to measure BACE1 activity using the assay kit according to the manufacturer's instructions, as described earlier.[39] The fluorescence was measured at an excitation wavelength of 345 nm and an emission wavelength of 500 nm, and the specific activity of the enzyme was determined by incubating parallel samples with a BACE1 inhibitor included in the assay kit. All samples were assayed in duplicate (two technical replicates).

2.10 | ELISA

The levels of soluble and insoluble human A$\beta_{1\text{-}40}$ and A$\beta_{1\text{-}42}$ in the frontal cortex and hippocampal homogenates of CSF- and PLGA-treated 5xFAD and WT mice (four or five mice per group) were determined using commercially available ELISA kits, as described previously.[29,39] Briefly, cortical and hippocampal tissues were homogenized in ice-cold homogenization buffer and centrifuged at 13,000 × g (4°C) for 10 min. The resulting supernatants were collected for quantification of soluble Aβ species. The corresponding pellets were dissolved in guanidine hydrochloride (GuHCl) buffer to extract the insoluble Aβ fractions. Both soluble and insoluble A$\beta_{1\text{-}40}$ and A$\beta_{1\text{-}42}$ were quantified using the human A$\beta_{1\text{-}40}$ and A$\beta_{1\text{-}42}$ ELISA kits, following the manufacturer's instructions. The pellets of the tissue homogenates prior to GuHCl extraction were used for the measurement of GFAP and synaptophysin levels using the respective mouse ELISA kits according to the manufacturer's instructions. The corresponding protein concentrations were normalized to pg/mg tissue using the following formula: Protein concentration (pg/mg tissue) = (ELISA output in pg/mL) × Dilution factor ÷ (Tissue mass [mg] ÷ Homogenization volume [mL]). The dilution factor corresponds to the total dilution of the original homogenate applied to the assay wells.

2.11 | Oxyblot, cellular/mitochondrial ROS level, and MitoSOX imaging

Cultured neurons treated with Aβ and PLGA and respective controls (described above) were used to determine carbonylated protein levels using the Oxyblot™ protein oxidation kit as described earlier.[28] All blots were re-probed with anti-β-actin to control for differences in protein loading. In parallel, the intracellular ROS levels in cultured neurons were examined by using the DCFDA/H_2DCFDA assay kit according to the manufacturer's instructions. The cell-permeable H_2DCFDA gets deacetylated by cellular esterases to form H_2DCF (a non-fluorescent compound), which is later oxidized by intracellular ROS to form fluorescent DCF, thereby serving as an indicator for ROS levels. In brief, control and Aβ-treated cultured cortical neurons with or without PLGA treatment for 24 h were exposed to 30 µM H_2DCFDA for 30 min at 37°C. Subsequently, cells were solubilized with PBS containing 1% SDS, and DCF fluorescence was measured at 485 nm excitation and 525 nm emission by a spectroscopic microplate reader.[40] Additionally, we measured mitochondrial ROS (mtROS) levels using a specific fluorescent probe, MitoSOX Red, along with a mitochondria-specific fluorogenic dye, MitoTracker™ Green FM, as described earlier.[41] The

fluorescence intensity of MitoSOX Red and MitoTracker Green were measured at 510 nm/580 nm and 490 nm/516 nm, respectively, using a SpectraMax M5 spectrophotometer (Molecular Devices, CA, USA). For cellular imaging, control and treated neurons plated on chamber slides following exposure to MitoSOX Red were mounted with ProLong Gold anti-fade reagent with DAPI and imaged using a Nikon Eclipse 90i fluorescence microscope with a Retiga 2000R Q imaging system (Nikon Instruments Inc.).

2.12 | SOD activity assay

The frontal cortex and hippocampus of 5xFAD and WT control mice treated with CSF or PLGA (three to five mice/group) were processed to measure SOD activity using the assay kit according to the manufacturer's instructions. In brief, brain tissues were homogenized using 0.1 M Tris/HCl buffer (pH 7.4), centrifuged at 13,000 × g for 10 min to obtain a supernatant fraction enriched with cytosol and mitochondria, which was then incubated with the reaction mix in parallel with SOD standard included in the assay kit. The enzymatic reaction was measured at 450 nm, and SOD activity was expressed as a percentage of the corresponding control. In parallel, to evaluate neuronal DNA damage due to oxidative stress along with Aβ-containing neuritic plaques, brain sections from CSF- and PLGA-treated 5xFAD and WT mice were double-immunolabeled with anti-8-OHdG (8-hydroxy-2′-deoxyguanosine) and fibrillar Aβ (OC) antibodies, and the sections were imaged using Nikon Eclipse 90i fluorescence microscope with a Retiga 2000R Q imaging system (Nikon Instruments Inc.).

2.13 | Semiquantitative analysis of immunostaining

To determine the number of neuritic plaques, immunolabeled cells, or their colocalization, cortical and hippocampal brain regions (three to five sections/mouse) from CSF- and PLGA-treated 5xFAD mice (n = 3 to 5/group) were analyzed. Using fibrillar Aβ (OC) antibody-labeled brain sections, the size, number, and area occupied by neuritic plaques were quantified as described earlier.[29] The number of CD68-positive microglia and plaque-associated IBA1-positive microglia were analyzed from double immunolabeled sections in the cortex and hippocampus of CSF- and PLGA-treated 5xFAD mice. In parallel, IBA1-labeled microglia and GFAP-labeled astrocytes were quantified from the cortex and hippocampus of immunolabeled sections visualized using the glucose-oxidase detection method. All the quantifications were performed by image processing software (Image J), as described earlier.[42] In parallel, the colocalization profile of IBA1-positive microglia and ThS-stained neuritic plaques was determined in four areas of the cortex and hippocampus by "co-localization finder" plugin in ImageJ software, which is presented as scatter plot-2D intensity histograms as described previously.[43]

2.14 | Statistical analysis

All statistical analyses were performed using GraphPad Prism (GraphPad Software, Inc., CA, USA). Data are presented as mean ± standard error of the mean (SEM), and statistical significance was set at $p < 0.05$. Asterisks or other symbols indicate the following significances: $^{*}p < 0.05$, $^{**}p < 0.01$, $^{***}p < 0.001$; $^{\#}p < 0.05$, $^{\#\#}p < 0.01$, $^{\#\#\#}p < 0.001$; $^{\S}p < 0.05$, $^{\S\S}p < 0.01$, $^{\S\S\S}p < 0.001$. Cognitive and behavioral test results were obtained from 10 to 12 animals per group, while biochemical, anatomical, and cellular data were collected from three to six biological replicates, with each experiment performed in duplicate or triplicate. Appropriate statistical analyses (e.g., one-way, two-way, or three-way ANOVA with repeated measures), followed by relevant post hoc tests, were applied as described in the corresponding figure legends.

3 | RESULTS

3.1 | Native PLGA treatment attenuated cognitive impairments in 5xFAD mice

The 5xFAD mice recapitulate some of the cardinal features of AD, including cognitive deficits, Aβ-containing neuritic plaques, neuroinflammation, synaptic loss, and degeneration of neurons in selected brain regions.[28,44,45] In the B6SJL genetic background, 5xFAD mice exhibit intraneuronal and extracellular amyloid accumulation starting from 1.5 to 2 months, with the manifestation of synaptic loss and cognitive/behavioral impairments, including spatial working memory, from 4 months onward. To evaluate the effects of native PLGA on AD-associated cognitive deficits and disease pathology, we chronically treated 8-month-old WT and 5xFAD male mice with PLGA for 28 days. At the end of the treatment period, we performed behavioral tests to examine learning and memory, as depicted in Figure 1A (created in BioRender). Chronic ICV administration of native PLGA for 28 days did not present any adverse clinical signs in mice, suggesting that PLGA at the given dose is relatively safe and nontoxic.

To determine whether PLGA can attenuate memory deficits in 5xFAD mice, we first performed the Morris water maze test to assess hippocampus-dependent spatial memory in WT and 5xFAD mice treated with or without native PLGA. The learning abilities of WT and 5xFAD mice were evaluated over 5 consecutive days based on their escape latencies to locate a submerged platform in a pool of opaque water. During the early phase (days 1 to 3) of the test, the two-way repeated measures ANOVA Dunnet's multiple-comparisons analysis revealed no significant difference among the groups. In the later days (days 4 and 5), however, the artificial CSF-treated 5xFAD mice demonstrated poor learning, as depicted by greater latency in finding the submerged platform (Figure 1B). Interestingly, 5xFAD mice treated with native PLGA showed a significant improvement, as represented by decreased latency to find the submerged platform compared to the CSF-treated 5xFAD mice, and it is somewhat similar to the per-

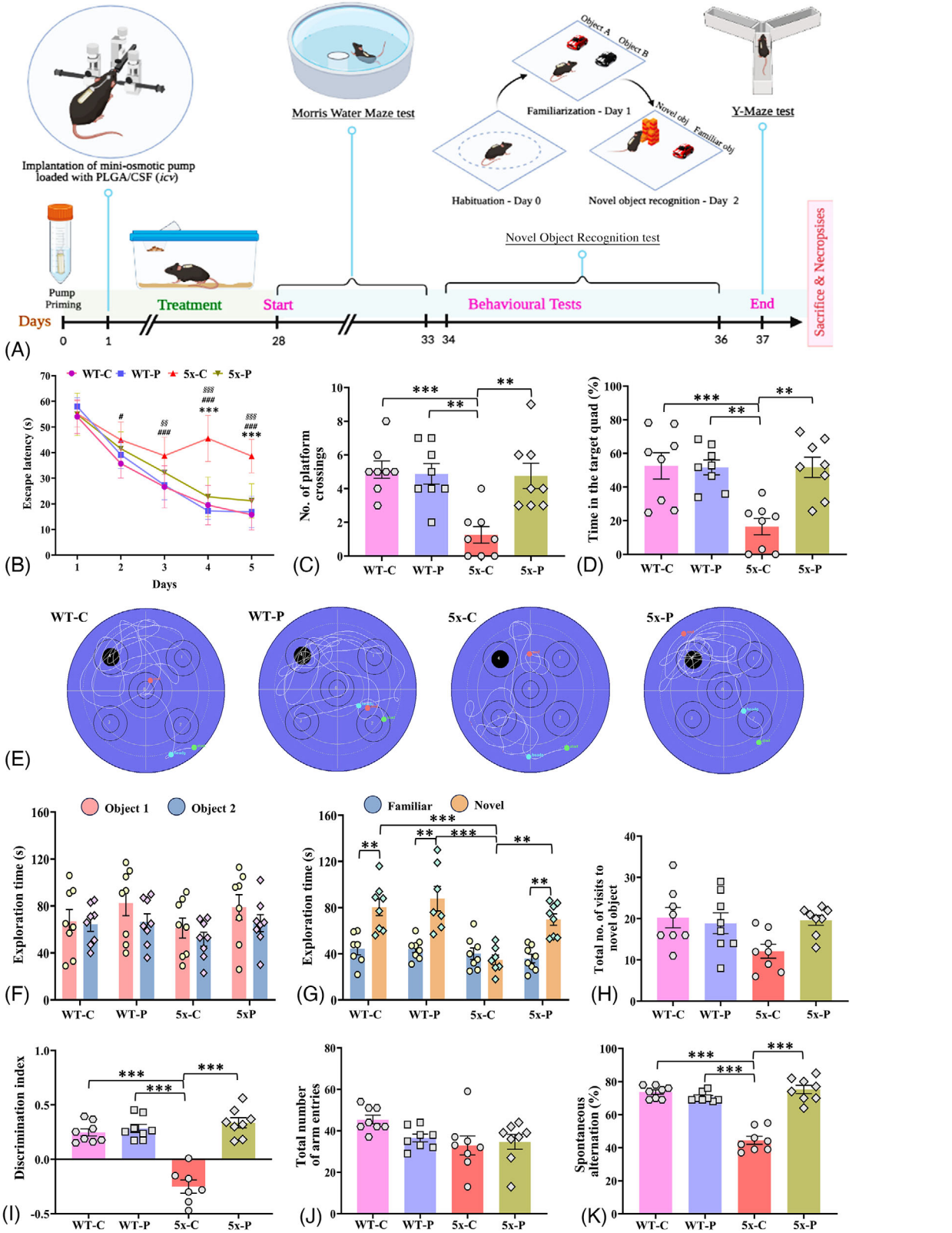

FIGURE 1 Native PLGA ameliorates cognitive deficits in 5xFAD mice. (A) Schematic representation showing experimental time frames of treatment and subsequent cognitive tests in CSF-/PLGA-treated control WT and 5xFAD mice (created in BioRender). (B–D) Morris water maze and probe test showing escape latencies and quadrant preferences in CSF-/PLGA-treated WT and 5xFAD mice. Note the significant cognitive impairment depicted in line graph of escape latencies during the training phase (B), bar plots with overlaid data points showing platform crossings (C), and target quadrant preference during probe trial (D) CSF-treated 5xFAD mice compared to CSF- and PLGA-treated WT mice and its improvement following PLGA treatment. (E) Morris water maze swimming traces recorded for CSF- and PLGA-treated WT and 5xFAD mice during probe trials. (F–I) Bar plots with individual scattered data points showing reversal of object recognition memory in 5xFAD mice following PLGA

formance of CSF-/PLGA-treated WT animals (Figure 1B). In the probe trial, performed 24 h after the last training session, two-way ANOVA Dunnet's multiple-comparisons analysis showed that the CSF-treated 5xFAD mice exhibited fewer crossings over the missing platform and spent less time in the target quadrant, reflecting impaired memory. In contrast, PLGA-treated 5xFAD mice exhibited a marked increase in platform crossings and the time spent in the target quadrant compared to the CSF-treated group (Figure 1C–E). During the training sessions, various additional parameters were assessed to evaluate motor and anxiety-like behaviors, including swimming speed and thigmotaxis, as well as probe trial metrics such as total swim distance and time spent in four different quadrants. None of the motor or anxiety-related parameters differed significantly between groups, indicating that the observed improvements were not due to changes in locomotor activity or anxiety-related behaviors. While total swim distance did not differ among four different groups, PLGA-treated 5xFAD mice, unlike CSF-5xFAD mice, were found to spend more time in target quadrant especially on day 5 as observed with CSF- and PLGA-treated WT mice, reflecting gradual learning progression over the 5-day training period (Figure S1A–G). Collectively, these results indicate that native PLGA treatment improved spatial learning in 5xFAD mice.

Subsequently, we performed the novel-object recognition memory test. In this test, the CSF-treated 5xFAD mice showed a reduced discrimination index toward a novel object compared to a familiar one, as reported earlier,[29] signifying an impaired recognition memory performance. The PLGA-treated 5xFAD mice, on the other hand, spent substantially more time exploring the novel object (higher discrimination index), indicating a significant improvement in non-spatial recognition and working memory compared to CSF-treated 5xFAD mice. The memory index of WT mice was not altered significantly following PLGA or CSF administration, as the total number of visits to the novel object or exploration time for both objects did not differ between the two groups. It is important to note that native PLGA treatment did not affect the exploratory activity of mice, which was similar between groups during the initial exposure and between trials (Figure 1F–I). Finally, we carried out the Y-maze test to evaluate the effects of native PLGA on the spatial working memory in 5xFAD mice, which exhibit impairment in their short-term memory from 4 months onward.[46,47] In this test, mice were allowed to explore freely the three arms of a Y-shaped maze, and their short-term spatial working memory was determined by the number of spontaneous alternations in arm entries on the Y-maze. The results showed a significant decline in the percentage of spontaneous alternations in 5xFAD mice compared to WT mice, which was attenuated following PLGA treatment. However, no differences were apparent in the alternation percentage between the CSF- and PLGA-treated WT mice or in the total number of arm entries among the four groups (Figure 1J,K).

3.2 | Native PLGA treatment reduced cerebral Aβ levels/deposit in 5xFAD mice

To determine whether chronic treatment with PLGA for 28 days could influence Aβ pathogenesis in 5xFAD mouse brains, we performed neuropathology analyses. We first assessed Aβ plaque load in the cortex and hippocampus of CSF- and PLGA-treated 5xFAD mice by immunolabeling with OC antibody (Figure 2A–I). Quantitative analysis of the amyloid burden with a two-way repeated ANOVA Sidak's multiple-comparisons tests revealed a significant decrease in the total number, average size, and area occupied by amyloid deposits in the cortex (i.e., frontal, parietal, and entorhinal regions) and hippocampus of the PLGA-treated 5xFAD mice compared to CSF-treated 5xFAD mice (Figure 2C–I). The attenuation of plaque load was validated using co-labeling of brain sections with ThS and Aβ immunostaining with 6E10 antibody (Figure S2A–L). No Aβ-containing neuritic plaques, as expected, were evident either in the cerebellum of 5xFAD mice (data not included) or in any brain region of CSF- or PLGA-treated WT mice (Figure 2A,B; Figure S2A–F). We also quantified Aβ levels in brain homogenates by ELISA and analyzed the results by two-way ANOVA Tukey's multiple comparisons. The analysis revealed a significant increase in the levels of both soluble and insoluble $A\beta_{1\text{-}40}$ and $A\beta_{1\text{-}42}$ as well as the ratio of $A\beta_{1\text{-}42}/A\beta_{1\text{-}40}$ in the cortex and hippocampus of 5xFAD mice compared to WT control mice. Chronic PLGA administration markedly attenuated the steady-state levels of soluble and insoluble $A\beta_{1\text{-}40}$ and $A\beta_{1\text{-}42}$ as well as the ratio of $A\beta_{1\text{-}42}/A\beta_{1\text{-}40}$ in the cortex and hippocampus of the 5xFAD mice compared to CSF-treated 5xFAD mice (Figure 2J–M; Figure S2 M,N). Interestingly, the levels of soluble $A\beta_{1\text{-}40}$ and $A\beta_{1\text{-}42}$ did not differ substantially either in the cortex or hippocampus of the CSF- and PLGA-treated WT mice (Figure 2J–M; Figure S2 M,N).

treatment compared to CSF- and PLGA-treated WT mice. The data represent the time spent exploring objects 1 and 2 during familiarization phase (F), time spent exploring familiar and novel objects in novel object recognition test (G), total number of visits to novel object (H), and discrimination index, calculated based on preference for novel object over familiar one (I). (J and K) Bar plots with overlaid data points showing attenuation of spatial working memory deficits in PLGA-treated 5xFAD mice compared to CSF- and PLGA-treated WT mice, as revealed by Y-maze test. Data represent number of arm entries (J) and percentage of spontaneous alternation (K) in Y-maze test. Data shown as mean ± SEM ($n = 10–12$ animals/group). Line graph and bar plots: (B) Two-way ANOVA with Dunnet's post hoc multiple-comparisons test (WT-C vs 5X-C is #; WT-P vs 5X-C is §; 5x-P vs 5X-C is *); (C,D, H, I, J, K) One-way ANOVA with Tukey's post hoc multiple-comparisons test; (F and G) Two-way ANOVA with Tukey's post hoc multiple-comparisons test. $p < 0.05$ considered significant. $^{*}p < 0.05$, $^{**}p < 0.01$, $^{***}p < 0.001$ or $\#p < 0.05$, $\#\#p < 0.01$, $\#\#\#p < 0.001$ or $\S p < 0.05$, $\S\S p < 0.01$, $\S\S\S p < 0.001$. CSF, cerebrospinal fluid; PLGA, poly(D,L-lactic-co-glycolic acid); SEM, standard error of the mean; WT, wild type.

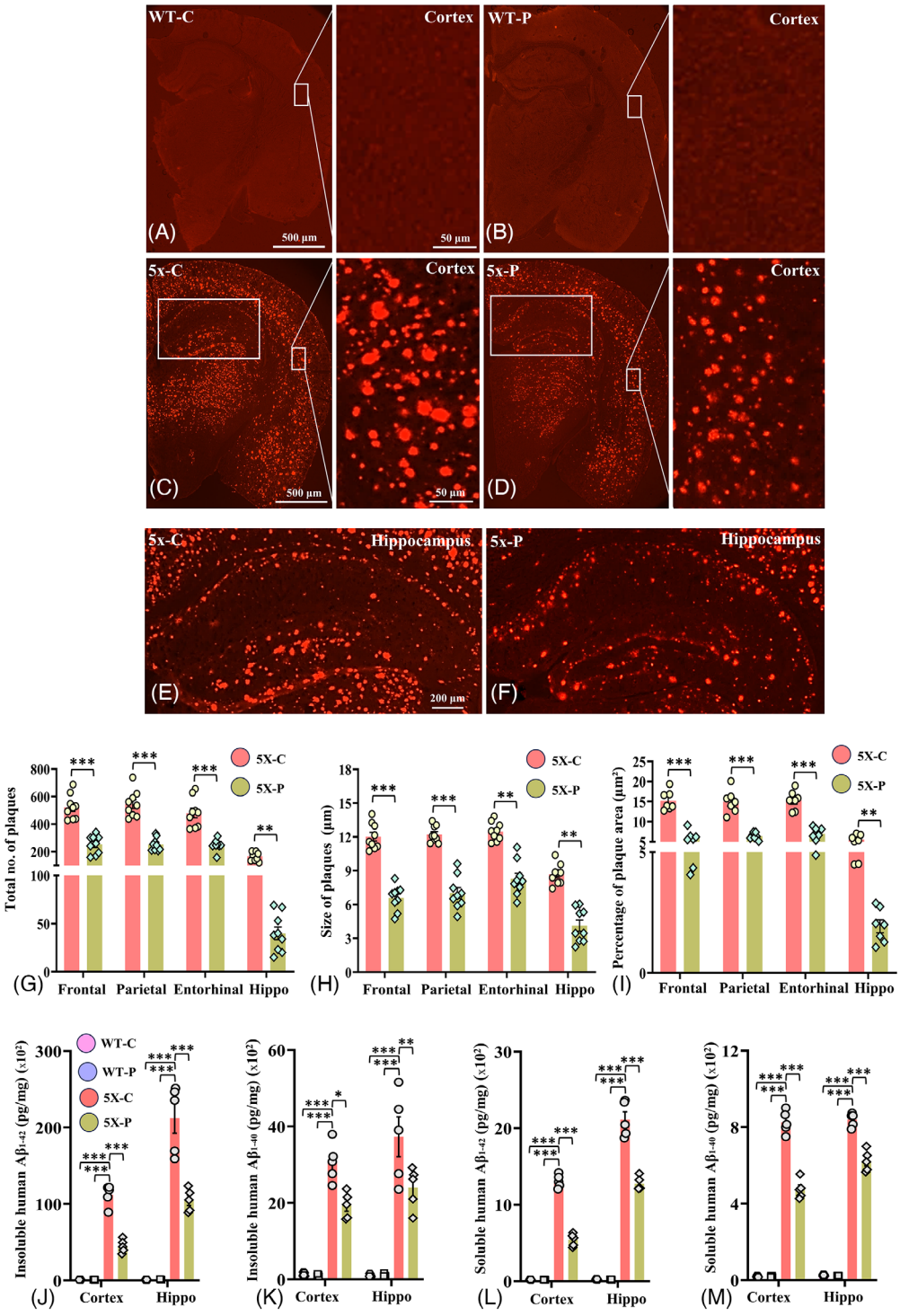

FIGURE 2 Native PLGA attenuates Aβ levels/accumulation in 5xFAD mice. (A–F) Photomicrographs depicting OC antibody labeled Aβ deposits in cortex and hippocampus of CSF-/PLGA-treated WT (A, B) and 5xFAD (C–F) mouse brain tissues. As expected, Aβ deposits are evident in the 5xFAD but not in WT mouse brain tissues. (G–I) Bar plot with scattered data points showing quantification of OC antibody labeled Aβ plaque number (G), plaque size (H), and percentage of area occupied by plaques (I) in frontal, parietal, and entorhinal cortical regions, as well as the hippocampus of PLGA-treated 5xFAD mice compared to CSF-treated 5xFAD mice. Note the decreased number, size, and areas occupied by Aβ-containing neuritic plaques in PLGA-treated 5xFAD mice compared to CSF-treated 5xFAD mice. (J–M) Bar plots with overlaid data points depicting decreased cortical and hippocampal levels of insoluble A$\beta_{1\text{-}42}$ (J) and A$\beta_{1\text{-}40}$ (K), as well as soluble A$\beta_{1\text{-}42}$ (L) and A$\beta_{1\text{-}40}$ (M), in PLGA-treated 5xFAD mice compared to CSF-treated 5xFAD mice. Data shown as mean ± SEM. Bar plots: (G–I) Two-way ANOVA with Sidak's post hoc multiple-comparisons test ($n = 3$ animals/group with data from three areas [per µm^2]); (J–M) Two-way ANOVA with Tukey's post hoc multiple-comparisons test ($n = 5$ animals/group; two technical replicates). $p < 0.05$ considered significant. $^*p < 0.05$, $^{**}p < 0.01$, $^{***}p < 0.001$. Aβ, amyloid beta; CSF, cerebrospinal fluid; OC, conformation-dependent anti-fibrillar Aβ antibody; PLGA, poly(D,L-lactic-co-glycolic acid); SEM, standard error of the mean; WT, wild type.

3.3 | Native PLGA treatment altered levels of APP and its processing enzymes in 5xFAD mice

To assess whether alterations in Aβ deposits/levels were the consequence of altered levels and/or processing of APP, we first determined the levels of APP holoprotein and its cleaved products in the cortex and hippocampus of CSF- and PLGA-treated WT and 5xFAD mice (Figure 3A–F; Figure S3A–F). Consistent with previous reports,[48,49] the levels of APP holoprotein and its cleaved products (i.e., α-CTF, β-CTF, sAPPα, and sAPPβ) were significantly increased in the cortex and hippocampus of 5xFAD mice compared to age-matched WT mice. Interestingly, native PLGA treatment decreased the levels of APP, α-CTF, β-CTF, sAPPα, and sAPPβ in the cortex and hippocampus of 5xFAD mice. Moreover, the ratios of CTFs/APP were also modestly decreased by PLGA treatment (Figure S3E,F). However, no differences between CSF- and PLGA-treated WT mice were observed in the steady-state levels of endogenous APP and its cleaved products (i.e., α-CTF, β-CTF, sAPPα, and sAPPβ) or the ratio of CTFs/APP in the cortex or hippocampus (Figure 3A–F; Figure S3A–F). Further, to determine whether the decreased levels of APP and its cleaved products in PLGA-treated 5xFAD mouse brains were the consequence of altered levels/activity of APP processing enzymes, we measured the levels of ADAM10, BACE1, and two components of γ-secretase complex (i.e., PS1 and nicastrin) as well as BACE1 activity in CSF-/PLGA-treated WT and 5xFAD mice (Figure 3G–L; Figure S3G,H). Interestingly, enhanced levels (Figure 3G–J) and activity (Figure 3K,L) of BACE1 observed in the cortex and hippocampus of 5xFAD mice compared to WT mice were found to be significantly attenuated following PLGA treatment. However, no alterations in ADAM10, PS1, or nicastrin levels were apparent in the cortex or hippocampus of PLGA-treated 5xFAD mice compared to CSF-treated 5xFAD mice. Additionally, PLGA treatment did not influence the levels of ADAM10, BACE1, PS1, or nicastrin in any brain regions of WT mice (Figure 3G–J; Figure S3G,H). Under the circumstances, it will be of interest to determine whether the decreased levels of α-CTF observed in 5xFAD mice after PLGA treatment result from lysosomal degradation or reduced activity of an α-secretase other than ADAM10.

3.4 | Native PLGA treatment attenuates synaptic deficits in 5xFAD brains

Earlier studies reported that loss of synapses and neurons, as in human AD pathology, is evident in the vulnerable regions of the 5xFAD mouse brain.[44,45] To determine whether PLGA treatment can influence synaptic density, we evaluated the levels/expression of presynaptic marker synaptophysin in the cortex and hippocampus of 5xFAD and WT mice with or without PLGA treatment (Figure S4A–K). Our results showed that synaptophysin levels, as detected using ELISA and Western blot analyses, decreased significantly in the cortex and hippocampus of 5xFAD mice compared to WT mice. However, this decrease was markedly attenuated following PLGA treatment. Native PLGA did not affect the levels of synaptophysin either in the cortex or hippocampus in WT mice (Figure S4A–C). These findings are in line with reduced synaptophysin immunoreactivity observed in brain slices from CSF-/PLGA-treated WT and 5xFAD mice (Figure S4D–K). The levels of post-synaptic marker PSD95 also showed a marked decrease in the cortex and hippocampus of 5xFAD mice compared to WT controls but was not found to be altered following PLGA treatment in either the 5xFAD or WT mice (Figure S4L,M). In parallel, we labeled brain sections with Fluoro-Jade C, a poly-anionic fluorescent dye that recognizes degenerating neurons and processes as well as Aβ-enriched-dense plaque cores (Figure S5A–L). Consistent with earlier results,[50] Fluoro-Jade C labeling was clearly present in the 5xFAD but not in WT (Figure S5) mouse brains. PLGA treatment somewhat decreased Fluoro-Jade C labeling in the cortex of 5xFAD mice compared to CSF-treated 5xFAD mice (Figure S5G–L).

3.5 | Native PLGA treatment in 5xFAD mice induces transcriptomic changes related to the immune response

To gain molecular insights and identify transcriptional changes induced by the PLGA treatment, we performed bulk RNAseq on cortical and hippocampal tissues of 8-month-old 5xFAD mice and age-matched controls treated with native PLGA or artificial CSF. RT-qPCR of human *PSEN1* and normalized counts for the *Thy1* promoter region were used to verify the genotypes of all RNA samples (Figure S6A,B). After quality control and filtering (see Methods), the purity-filtered reads ranged from 48 to 79 M per library (Figure S6C). The basic statistics for all genes across multiple samples, shown as boxplot and density plot (Figure S6D), revealed an overall similar distribution, with no outliers. PCA comparison of the overall brain transcriptome revealed that the first principal component accounted for 20% of the total variance and separated the mice by genotype into the 5xFAD and WT groups. The second principal component accounted for 11% of the total variance and separated PLGA treatment only in the 5xFAD cohort, indicating a genotype-specific response to PLGA (Figure 4A). We compared the overall dataset composed of 16,496 transcripts in the CSF WT, 17,135 in the CSF 5xFAD, 17,010 in the PLGA WT, and 17,155 in the PLGA 5xFAD using an upset plot to identify common and unique transcripts across the groups (Figure 4B). Next, we focused on the 601 transcripts uniquely expressed in PLGA-treated 5xFAD mice and not in the other three groups (Figure 4B) and examined them by GO analysis. The top enriched GO terms included regulation of immune effector processes, positive regulation of response to external stimulus, and lymphocyte-mediated immunity (Figure 4C). Gene signature partitioning of DEGs revealed 284 shared DEGs between 5xFAD and WT in either PLGA treatment or CSF control (Figure 4D, overlapping region in Venn diagram on left). Intriguingly, PLGA treatment resulted in distinct gene expression changes in 5xFAD (129 DEGs) and WT mice (123 DEGs) (Figure 4D, Venn diagram on right), with no shared DEGs. PLGA treatment resulted in enriched unique DEGs in 5xFAD compared to WT

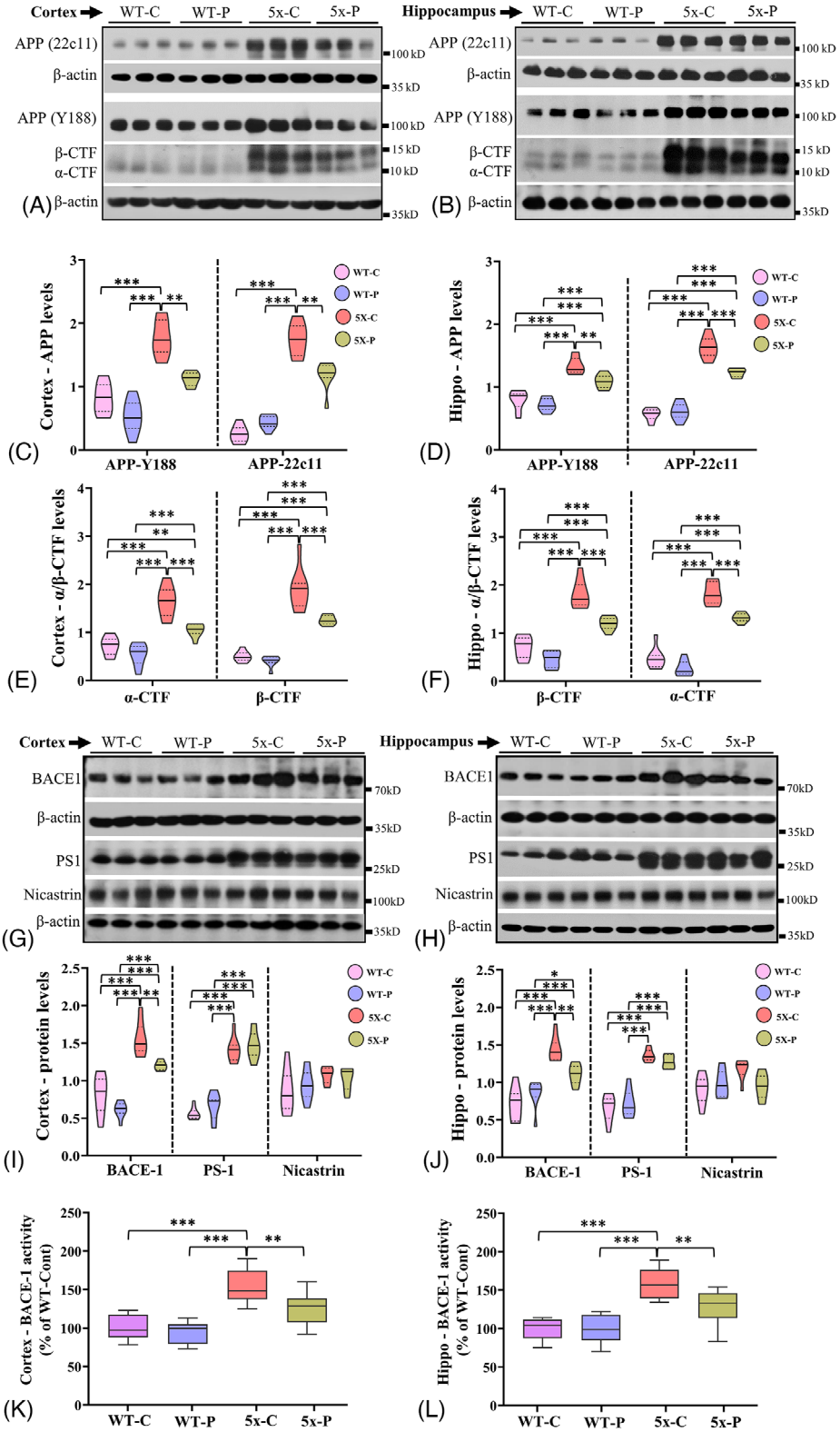

FIGURE 3 Native PLGA alters APP levels and processing enzymes in 5xFAD mice. (A–F) Immunoblots (A, B) and their quantifications (C–F) showing levels of APP holoprotein (22c11, Y188) and the corresponding C-terminal fragments (i.e., α-CTF and β-CTF) in the cortex (C, E) and hippocampus (D, F) of CSF-/PLGA-treated WT and 5xFAD mouse brain tissues. Note the decreased levels of APP and its cleaved products in the cortex and hippocampus of PLGA-treated 5xFAD mice compared to CSF-treated 5xFAD mice (C–F). (G–J) Immunoblots (G, H) and their quantifications (I, J) showing levels of APP processing enzymes – BACE1, PS1, and nicastrin in cortex (G, I) and hippocampus (H, J) of CSF-/PLGA-treated WT and 5xFAD mouse brains. Note the increased levels of BACE1 and PS1, but not nicastrin, in the cortex and hippocampus of 5xFAD mice compared to WT mice. PLGA treatment differentially affects the levels of BACE1 and PS1 in the cortex and hippocampus of 5xFAD mice compared to untreated mice. (K and L) Boxplots showing BACE1 enzyme activity in cortex and hippocampus of CSF-/PLGA-treated WT and 5xFAD mouse brain tissues. Note the increased activity of BACE1 in 5xFAD mice compared to WT mice and its decline following PLGA treatment.

mice (618 DEGs under PLGA vs 78 DEGs under CSF condition). We then sought to verify the transcriptomic signatures of the amyloidosis model. Our analysis identified 614 genes differentially expressed between 5xFAD and WT, as illustrated in the volcano plot (Figure 4E). As expected,[32,51] *Tyrobp*, *Cd68*, *Trem2*, *Tbxas1*, *Clec7a*, *Ctsd*, *Itgax*, and *Cst7* were expressed at higher levels in the 5xFAD mice compared to non-transgenic controls. The top terms generated in a GO biological process analysis of the 614 DEGs were plotted in a dot plot (Figure S7A,B), confirming the activation of inflammatory pathways in the 5xFAD mice, consistent with previous reports.[52–54] We also examined the 129 DEGs identified when 5xFAD mice treated with PLGA were compared to 5xFAD CSF controls (Figure 4F). Among those DEGs, *Styx*, *Ifitm1*, *Ms4a6d*, *Cebpd*, and *Socs3* were top hits among upregulated genes, whereas *Dpysl15*, *Kcnc3*, and *Fgf16* were downregulated. Those DEGs were enriched for GO terms: leukocyte migration, cytokine-mediated signaling pathway, and cell chemotaxis (Figure S7C and D). These results show that PLGA treatment of 5xFAD mice influences immune response-related gene expression.

We further calculated the normalized enrichment score (NES) by GSEA. To interpret the GSEA results, a network-based and text-mining approach provided by VissE (R package) was used to cluster the significantly enriched pathways; 16 clusters were identified (Figure 5A–C). Clusters 1, 2, 3, 4, 7, 9, 10, and 12 showed a theme of immune response or inflammatory response (Figure 5B), and the representative gene set was immune response (Figure 5D). Cluster 16 emphasized the vesicle exocytosis functions. PLGA-treated 5xFAD showed a decreased NES score in regulating synaptic vesicle exocytosis gene set (Figure 5E). Cluster 14 contained the oxygen metabolic-related pathways, and Figure 5F represents the gene set for cellular oxidant detoxification.

3.6 | Native PLGA-treated 5xFAD leads to transcriptomic changes related to AD signatures

To further understand differential gene expression in 5xFAD mice in the context of co-expression networks, we performed WGCNA. This analysis identified 15 modules of co-expressed genes in the RNA-seq dataset displayed in different colors (Figure 6A). To assess how these genes may relate to known gene expression changes associated with human AD neuropathology, all modules from this study were compared to five previously identified consensus clusters (named Clusters A–E) that describe the major functional groups of alterations observed through meta-analysis in human AD.[55] Another way to check the treatment effect of 5xFAD-PLGA mice with the emerged modules is the eigengene adjacency matrix, which is shown as a heatmap (Figure S8A). From the eigengene adjacency matrix, we observed a correlation between the red and blue modules with the 5xFAD-PLGA group. The most pronounced correlations were observed in the blue module with the Consensus Cluster B (Figure 6B–D), which consists of immune system pathways, and the -green module with Cluster C, which consists of the gene functions in the neuronal system (Figure 6B–D). GO enrichment analysis of the green module showed pathways including regulation of membrane potential and exocytic process (Figure S8B). Gene significance (Figure S8C) and GO enrichment analysis (Figure S8D) for the -red module emphasized a translation-related function in the 5xFAD-PLGA group. GO enrichment analysis on the blue module is shown as a dot plot (Figure 6E). The enriched gene networks in the blue module are similar to immune response genes previously identified from GO analysis of unique transcripts (Figure 4C) and GSEA (Figure 5B). We then experimentally verified eight DEGs from the blue module related to the immune response by RT-qPCR. We found significant upregulation of *Tyrobp*, *Csf1*, *P2ry12*, *Irf8*, *Cst7*, *Cst3*, *and Cd33* in 5xFAD mice. All these genes and *Timp2* levels were significantly increased further after PLGA treatment in 5xFAD mice relative to CSF controls (Figure 6F).

3.7 | Native PLGA treatment influences astrocytes and microglia activation in 5xFAD mice

Astrocytes and microglia play critical roles in the development and progression of AD pathology.[56,57] Consistent with earlier studies,[44,45,58] we observed an increase in the number and activation of astrocytes in the cortex and hippocampus of 5xFAD mice compared to age-matched WT controls (Figure S9A–E). Our Western blot and ELISA analyses also revealed a significant increase in GFAP levels in the cortex and hippocampus of 5xFAD mice compared to age-matched WT controls (Figure S9F–H). Interestingly, PLGA-treated 5xFAD mice showed a notable decrease in the number of astrocytes and the levels of GFAP in both cortex and hippocampus compared to CSF-treated 5xFAD mice. Native PLGA, however, did not markedly influence the astrocyte population or the levels of GFAP in WT mice (Figure S9A–H). In addition to astrocyte alteration, 5xFAD mice showed profound microglial activation in the cortex and hippocampus compared to age-matched WT mice. At the cellular level, IBA1-labeled microglia in WT mice displayed smaller cell bodies with a few ramified processes typical of resident microglia. In contrast, hypertrophic, amyloid-reactive microglia were apparent in the 5xFAD mouse brains (Figure 7A–E). Some activated microglia were found in close association with ThS-labeled neuritic plaques in 5xFAD mice (Figure S9I–O). Furthermore, Western blot analysis showed a significant increase in IBA1 levels in the cortex and hippocampus of 5xFAD mice compared to WT mice (Figure 7F,G). Chronic exposure of 5xFAD mice to PLGA decreased IBA1 steady-state levels and reduced the number of microglia, including those in prox-

Data are from four or five animals/group with two or three technical replicates. Violin and boxplots: (C–F, I, and J) Two-way ANOVA with Tukey's post hoc multiple-comparisons test; (K and L) One-way ANOVA with Tukey's post hoc multiple-comparisons test. $p < 0.05$ considered significant. $^{*}p < 0.05$, $^{**}p < 0.01$, $^{***}p < 0.001$. APP, amyloid precursor protein; BACE, β-site APP cleaving enzyme; CSF, cerebrospinal fluid; CTF, C-terminal fragment; PLGA, poly(D,L-lactic-co-glycolic acid); PS1, presenilin 1; WT, wild type.

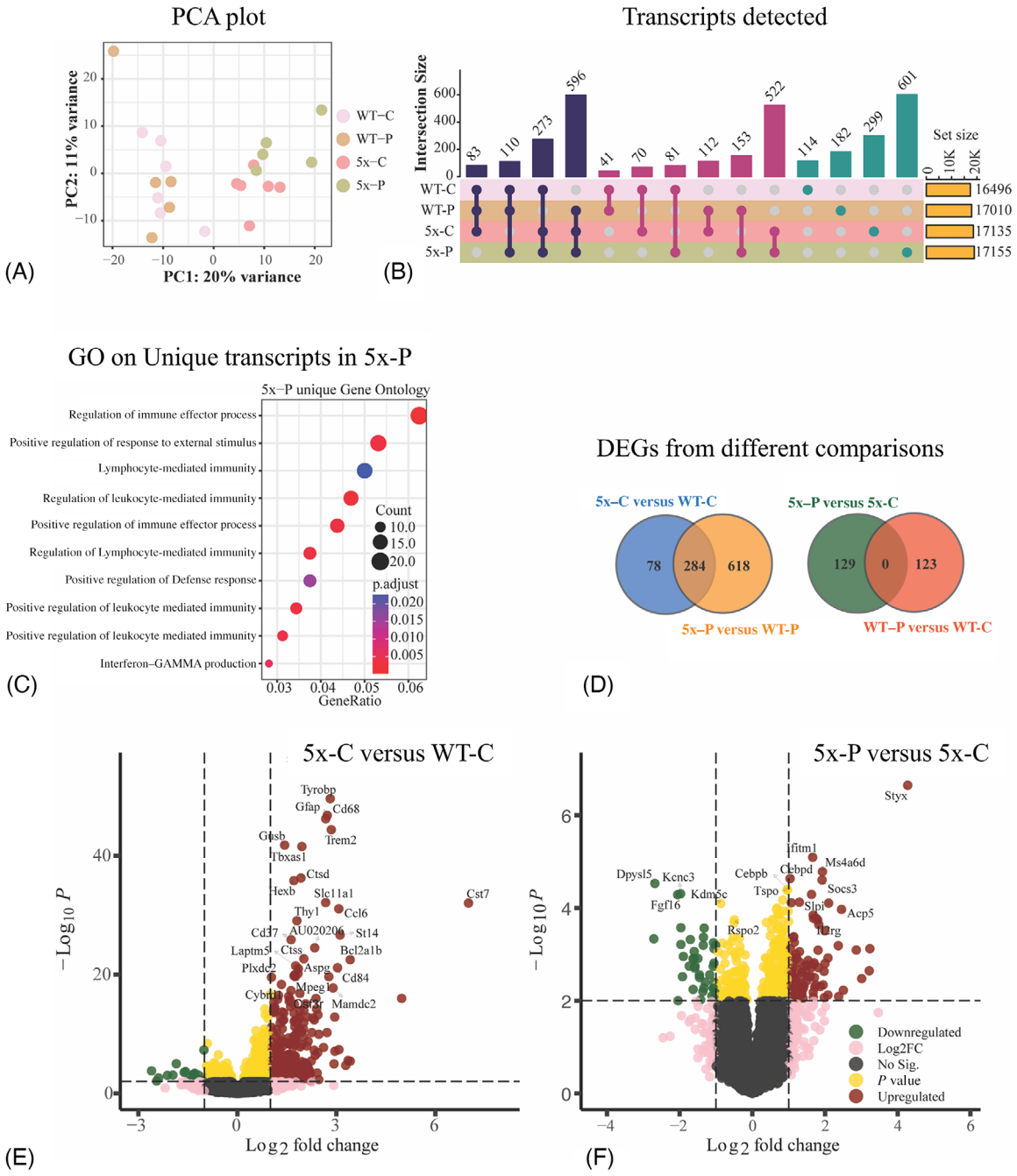

FIGURE 4 Transcriptomic analysis of WT and 5xFAD mice treated with PLGA. (A) Upset plot representing common and unique transcripts across the experimental groups. There were 16,496 transcripts expressed throughout all four groups. The number of unique transcripts of WT-CSF, WT-P, 5xFAD-CSF, and 5xFAD-PLGA was 114, 182, 299, and 601, respectively. (B) Principal component analysis for all genes detected in bulk RNAseq analysis. Principal components (PC) 1 and 2 account for 20% and 11% of the variance, respectively. (C) Top 10 enriched GO terms from 601 unique genes from 5xFAD-PLGA group. The 10 GO processes with the most significant adjusted *p* value are plotted in order of gene ratio. The color of the dots represents the adjusted *p* value with the GO term, and the size of the dots signifies the gene counts belong to the respective GO term. (D) Venn diagram of DEGs from 5xFAD-CSF versus WT-CSF with or without PLGA treatment is depicted on the left. DEGs from PLGA treatment in the context of 5xFAD or WT gene background are shown on the right. (E) Volcano plot of DEGs from comparison of 5xFAD-CSF and WT-CSF. The threshold for significance was set at $p < 10^{-2}$, and log2 (fold change) > 1. Color-coded symbols depict the fold change and *p* value below or above the thresholds. Green: $p < 10^{-2}$, and log2 (fold change) < −1; red: $p < 10^{-2}$, and log2 (fold change) > 1; pink: $p > 10^{-2}$, and | log2 (fold change) | > 1; gold: $p < 10^{-2}$, and |log2 (fold change) | < 1; gray: $p > 10^{-2}$, and | log2 (fold change) | < 1. (F) Volcano plot of DEGs from comparison between 5xFAD-PLGA and 5xFAD-CSF groups. The threshold and color coding are the same as (E). CSF, cerebrospinal fluid; DEG, differentially expressed gene; GO, Gene Ontology; PLGA, poly(D,L-lactic-co-glycolic acid); WT, wild type.

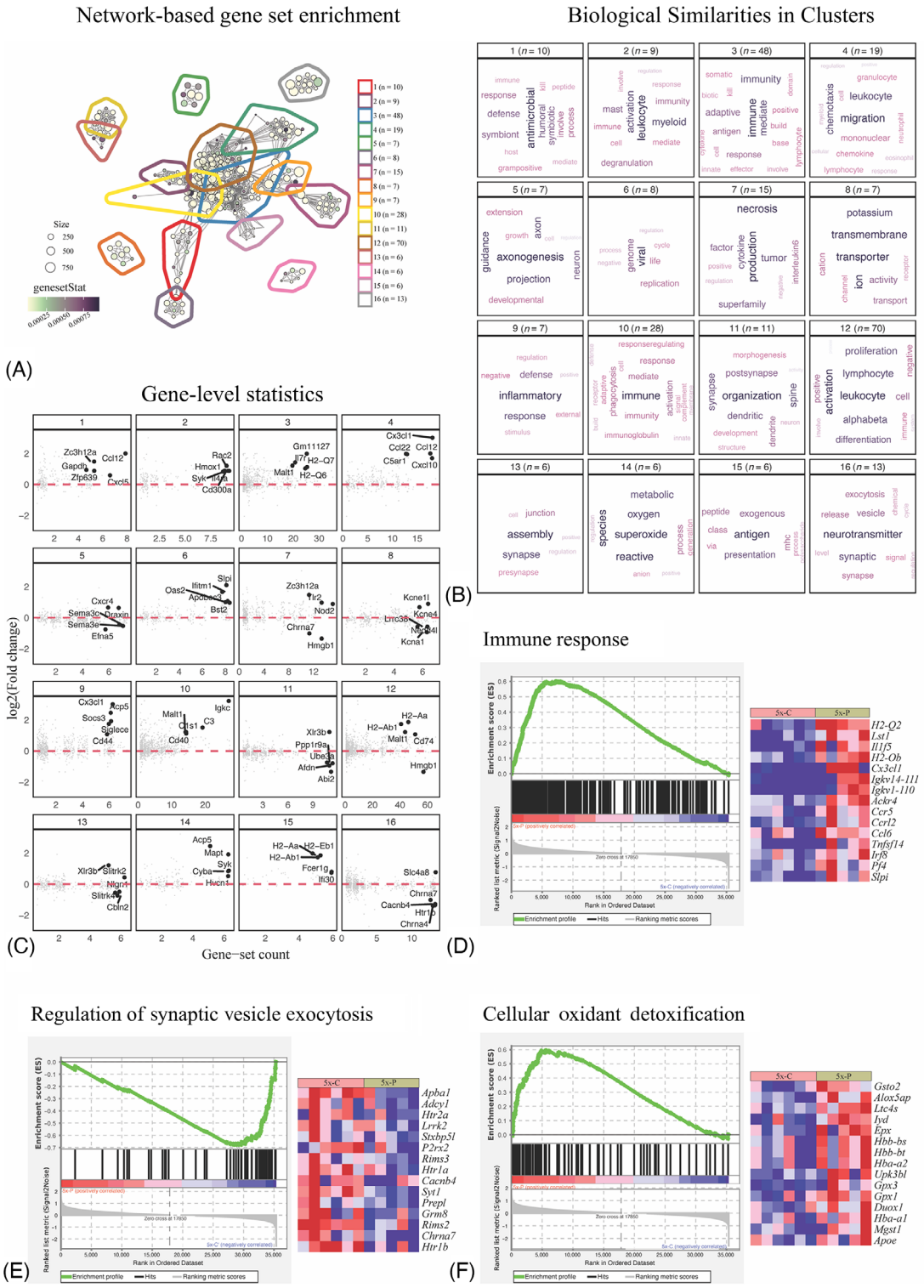

FIGURE 5 PLGA treatment regulates oxidase activity and immune response in 5xFAD mouse model. (A) Network-based gene set enrichment; 16 clusters were identified. (B) Biological similarities in the 16 clusters. Cluster annotations generated by text-mining analysis of gene-set names were shown as word clouds, and the size of each word represented the frequency appearing in the cluster. (C) Gene loadings (also known as weights): the log2 fold change (log2FC) of genes belonging to gene sets in the cluster is plotted against the number of gene sets to which the gene belongs. (D) Immune response. The gene set enrichment analysis (GSEA) plot shows the enrichment of immune response gene sets in the 5xFAD-PLGA group. The top 15 genes ordered by *p* value were plotted as a heatmap. Gradual red and blue colors represent the *z*-score of up- and downregulated genes. (E) Regulation of synaptic vesicle exocytosis. The plot shows the enrichment of regulation of synaptic vesicle exocytosis gene sets in the 5xFAD-PLGA group. The top 15 genes ordered by *p* value were plotted as a heatmap. (F) Cellular oxidant detoxification. The plot shows the enrichment of cellular oxidant detoxification gene sets in the 5xFAD-PLGA group. The top 15 genes ordered by *p* value were plotted as a heatmap.

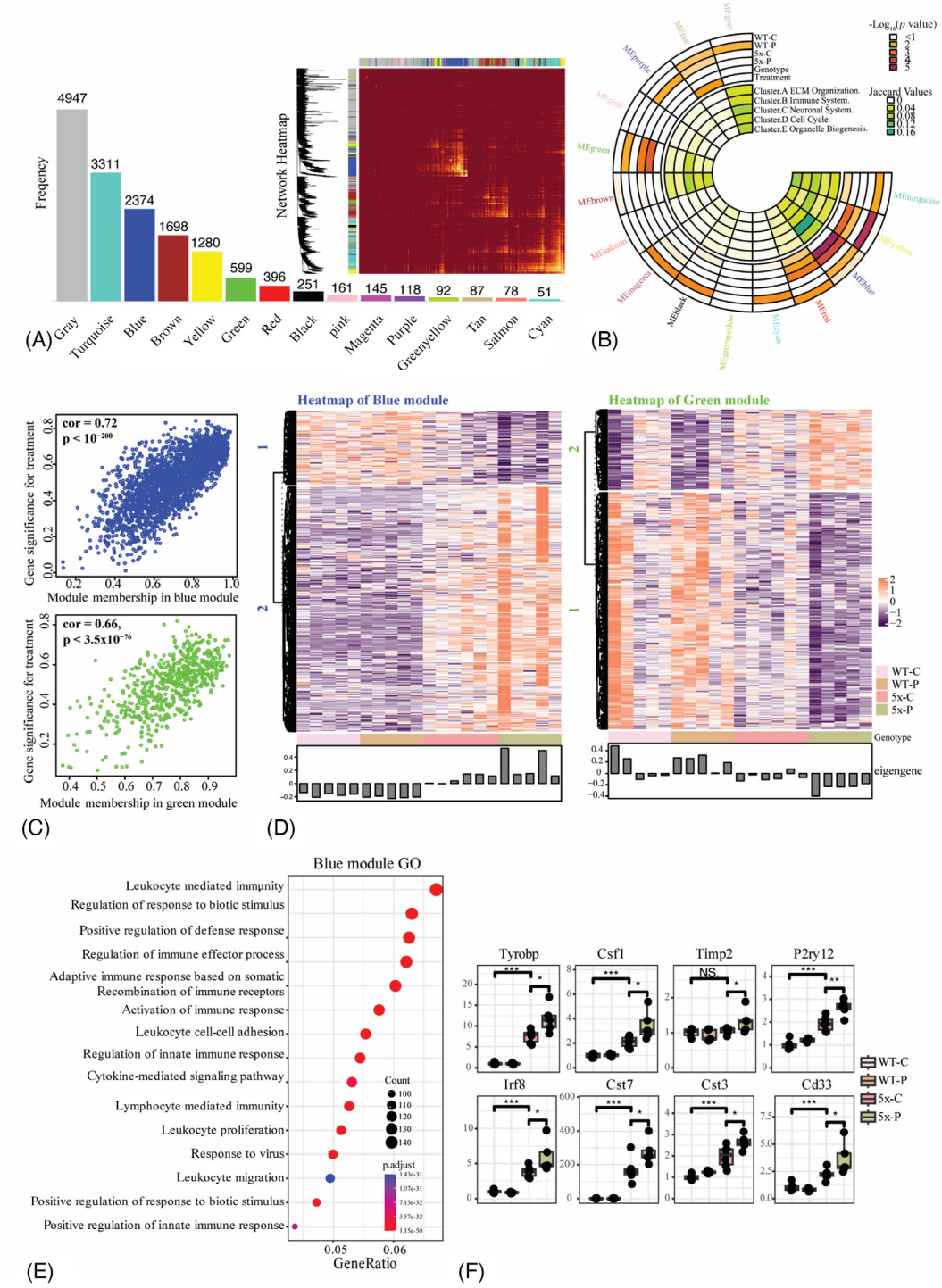

FIGURE 6 WGCNA and identification of immune and neuronal system-specific modules from AMP-AD. (A) An RNA co-expression network building by WGCNA consisted of 15 RNA co-expression modules, where gray stands for non-clustering genes. The size of each module is plotted as a bar graph, and the co-expression TOM is depicted as a heatmap. A low TOM value is indicated by red, and a progressively yellow color characterizes a higher TOM. (B) Circular heatmap of module–trait relationship and module–cluster Jaccard score. The negative log10 (p value) of each module–trait relationship is coded differently in red in the outer ring. The Jaccard value between modules defined in this study and AMP-AD is coded differently in green in the inner ring. (C) GS versus MM. The scatter plot represents the GS of the PLGA treatment and MM of the blue and green modules. (D) Heatmap of genes in blue and green modules. (E) The 15 GO processes of blue module with most significant adjusted p value plotted in order of gene ratio. Dot colors represent adjusted p value with GO term, and the size corresponds to gene counts in GO term. (F) RT-qPCR confirmation of immune-related gene expression. The y-axis represents the relative expression level normalized to *Gapdh* compared with the WT-CSF group. Data shown as mean ± SEM ($n = 5–6$ animals/group). One-way ANOVA with Tukey's post hoc multiple-comparisons test. $p < 0.05$ considered significant. *$p < 0.05$, **$p < 0.01$, ***$p < 0.001$. AMP-AD, accelerating medicines partnership® program for alzheimer's disease; GO, gene ontology; GS, gene significance; MM, module membership; RT-qPCR; quantitative reverse transcription polymerase chain reaction; TOM, topological overlap matrix; WT, wild type.

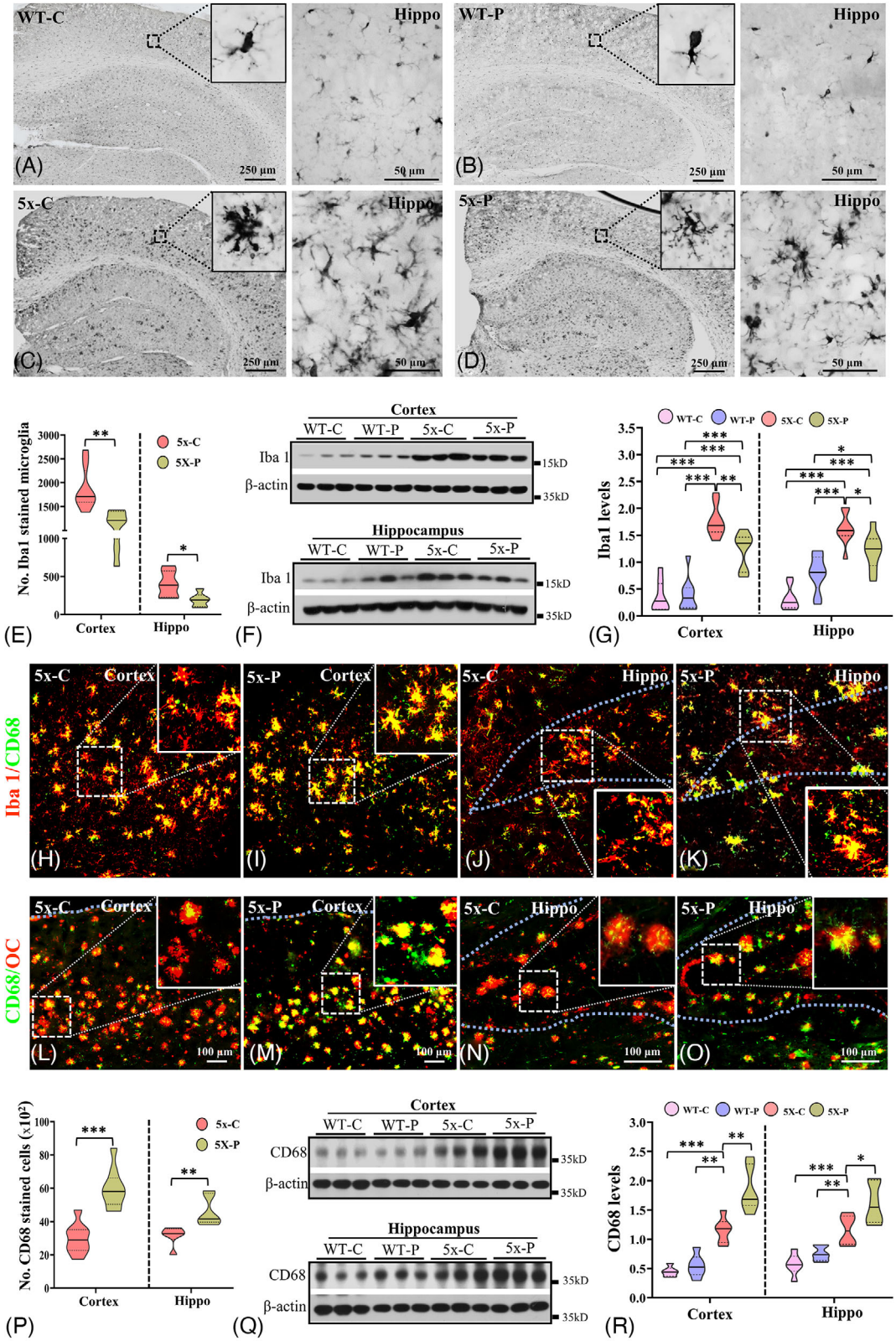

FIGURE 7 Native PLGA alters the levels of microglial markers in 5xFAD mice. (A–E) Photomicrographs showing IBA1-immunoreactive microglia in the cortex and hippocampus of CSF-/PLGA-treated WT (A, B) and 5xFAD (C, D) mouse brain tissues. Our semiquantitative analysis revealed an increase in IBA1-positive microglia in 5xFAD mice compared to WT mice. Note decrease in number of microglia in cortex and hippocampus of PLGA-treated 5xFAD mice compared to CSF-treated 5xFAD mice (E). (F and G) Immunoblots (F) and their quantifications (G) showing levels of IBA1 in cortex and hippocampus of CSF-/PLGA-treated WT and 5xFAD mouse brains. Note increase in levels of IBA1 in 5xFAD mice compared to WT mice and its decrease following PLGA treatment in 5xFAD mice. (H–K) Photomicrographs showing double immunolabeling of IBA1 (red) and disease-associated microglia marker CD68 (green) in cortex (H, I) and hippocampus (J, K) of CSF-/PLGA-treated 5xFAD mouse brains. (L–O) Photomicrographs showing double immunolabeling of OC (red) and CD68 (green) in cortex (L, M) and hippocampus (N, O) of

imity to the ThS-labeled neuritic plaques (Figure 7A–E; Figure S9I–O). Intriguingly, the population of IBA1-labeled microglia or the steady-state expression of IBA1 was not altered in WT mice following PLGA treatment (Figure 7A–G).

Next, we analyzed CD68, a protein primarily localized in the lysosomes of activated microglia, to study the potential role of microglia in Aβ clearance following PLGA treatment. Earlier studies showed that CD68-labeled dystrophic microglia were present in the vicinity of neuritic plaques, representing microglial phagocytosis in AD pathology.[46,59–61] In agreement with this, IBA1-labeled microglia in the cortex and hippocampus of 5xFAD mice were positive for CD68 (Figure 7H–K). Interestingly, in contrast to IBA1, the intensity of CD68 immunoreactivity appeared to be enhanced in PLGA-treated 5xFAD mice compared to CSF-treated 5xFAD mice (Figure 7H–K). Since CD68-positive microglia are mostly found adjacent to Aβ-containing neuritic plaques, we subsequently evaluated CD68 immunoreactivity in relation to OC antibody-labeled neuritic plaques in 5xFAD mice with or without PLGA treatment. Our results revealed that the number of CD68-positive microglia was also enhanced in the cortex and hippocampus of PLGA-treated 5xFAD mice in comparison to CSF-treated 5xFAD mice (Figure 7L–P). The densitometric analysis of the core form of the CD68 was concurrently increased not only in the 5xFAD mice compared to WT mice but also in PLGA-treated 5xFAD mice in relation to untreated 5xFAD mice (Figure 7Q,R). The rise in CD68 expression in the PLGA-treated 5xFAD mice suggests an overall increase in microglial lysosomal pathway/activity, which is supported by the enrichment of gene sets for response to external stimulus (Figure 4C) and regulation of immune response (Figures 5B and 6E). In fact, some earlier studies in 5xFAD-Tg mice showed that impaired phagocytosis followed by decreased lysosomal clearance of Aβ-related peptides was associated with the development of disease pathology, while enhanced phagocytosis and lysosomal clearance of Aβ could mitigate disease pathology.[46,62,63]

3.8 | Native PLGA treatment suppresses markers of oxidative stress in Aβ-treated neurons and in 5xFAD mice

Multiple lines of experimental data suggest that oxidative stress, represented by an imbalance between antioxidant defense and production of toxic free radicals, plays a critical role in Aβ-mediated toxicity as well as in AD pathogenesis.[64,65] Consistent with these results, we found that Aβ treatment substantially increased the intracellular and mitochondrial ROS levels in mouse cortical cultures compared to untreated control neurons (Figure 8A–H). This was evident not only by Oxyblot analysis depicting higher levels of carbonylated proteins and ROS levels (Figure 8A–C) but also with MitoSox labeling, indicating a higher amount of superoxide generation within mitochondria in Aβ-treated cultured neurons (Figure 8D–H). Intriguingly, native PLGA treatment significantly reduced intracellular and mitochondrial ROS levels in Aβ-treated cortical cultured neurons without influencing ROS levels in untreated control neurons (Figure 8A–H). Accompanying cultured neurons, we evaluated whether native PLGA could influence oxidative stress markers in the cortex and hippocampus of 5xFAD and WT mice. Our results clearly showed that while the levels and activity of antioxidant enzyme SOD2 were markedly decreased (Figure 8I–K), the expression of oxidative marker OH8dg was enhanced in the cortex and hippocampus of 5xFAD mice compared to WT mice (Figure 8L–P). Interestingly, PLGA treatment significantly enhanced SOD2 levels/activity and decreased expression of the oxidative marker OH8dg in both the cortical and hippocampal regions of 5xFAD mice but not in WT mice (Figure 8L–P). Apart from ROS, reactive nitrogen species and products of lipid peroxidation and protein oxidation such as peroxynitrite, nitrotyrosine-modified proteins, advanced glycation end products, and aldehydes have also been involved in the degeneration of neurons in AD brains.[66–68] Thus, it would be of clinical relevance to determine whether native PLGA could influence the functions of these markers together with the overall redox imbalance to define its implications in regulating broader groups of free radicals known to contribute to the development and progression of AD.

4 | DISCUSSION

In this study, we report that chronic ICV administration of native PLGA nanoparticles can attenuate cognitive deficits and disease pathology in 8-month-old male 5xFAD mouse model of AD. Results from multiple approaches demonstrate that native PLGA can (i) reverse cognitive deficits; (ii) decrease cerebral Aβ burden concomitant with a reduction in APP and its metabolites (α-CTF, β-CTF, sAPPα, sAPPβ); (iii) attenuate BACE1 levels/activity without affecting the levels of ADAM10 or γ-secretase subunits (PS1 and nicastrin); (iv) diminish synaptic loss and Fluoro-Jade C-labeled degenerative structures; (v) induce transcriptional changes in genes involved in vesicle exocytosis, immune responses, and oxidative stress; (vi) alter glial activation that may involve lysosomal Aβ clearance; and (vii) mitigate oxidative stress. Collectively, these results underscore the therapeutic potential of native PLGA nanoparticles in treating AD-related pathology.

CSF-/PLGA-treated 5xFAD mouse brains. (P) Our semiquantitative analysis revealed an increase in the number of CD68-labeled microglia in the cortex and hippocampus of PLGA-treated 5xFAD mice compared to CSF-treated 5xFAD mice. (Q and R) Immunoblots (Q) and their quantifications (R) showing levels of CD68 in cortex and hippocampus of CSF-/PLGA-treated WT and 5xFAD mouse brains. Note increase in levels of core CD68 in 5xFAD mice compared to WT mice and its enhancement following PLGA treatment in 5xFAD mice. Data shown as mean ± SEM ($n = 3–4$ animals/group with two or three technical replicates). Violin plots: (E and P) -Paired *t*-test; (G and R) Two-way ANOVA with Tukey's post hoc multiple-comparisons test. $p < 0.05$ considered significant. $^{*}p < 0.05$, $^{**}p < 0.01$, $^{***}p < 0.001$. CSF, cerebrospinal fluid; IBA1, Ionized calcium-binding adapter molecule 1; PLGA, poly(D,L-lactic-co-glycolic acid); WT, wild type.

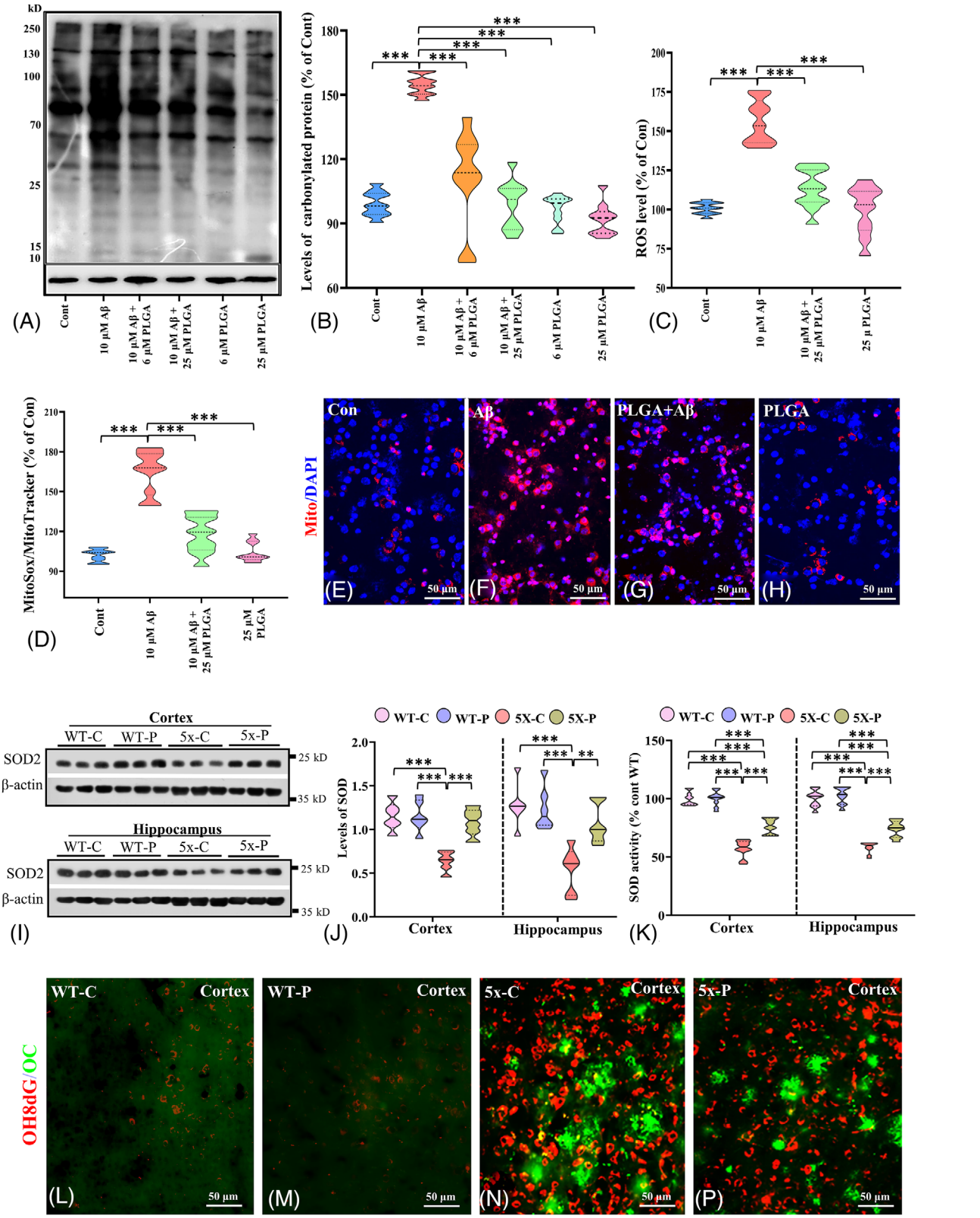

FIGURE 8 Native PLGA alters oxidative stress in Aβ-treated cultured neurons and 5xFAD mice. (A and B) Immunoblot (A) and corresponding violin plot (B) showing increased levels of carbonylated proteins in A$\beta_{1\text{-}42}$-treated mouse cortical cultured neurons and their decrease following PLGA treatment. (C) Violin plots depicting an increase in cellular ROS (DCFDA) level in A$\beta_{1\text{-}42}$-treated cortical cultured neurons and its decrease following PLGA treatment. (D–H) Violin plots and photomicrographs showing mitochondrial ROS (Mitosox Red) levels (D) and its expression (E–H) in A$\beta_{1\text{-}42}$-treated cortical cultured neurons and its decrease following PLGA treatment. Cultured neurons were labeled with DAPI (blue) to identify neuronal nuclei. (I and J) Immunoblots (I) and their quantifications (J) showing levels of antioxidant enzyme Superoxide Dismutase 2 (SOD2) in the cortex and hippocampus of CSF-/PLGA-treated WT and 5xFAD mouse brains. Note the decreased levels of SOD2 in 5xFAD mice compared to WT

PLGA nanoparticles have long been used to deliver potential drugs and therapeutic agents for various neurodegenerative diseases, including AD.[69] In fact, PLGA nanoparticles encapsulated with a variety of phytochemicals, acetylcholinesterase inhibitors, growth factors, and hormones have demonstrated beneficial effects in cellular/animal models of AD by inhibiting Aβ aggregation/toxicity.[20–24,70,71] In contrast to the drug-conjugated PLGA, this study reveals that native PLGA can attenuate spatial and non-spatial cognitive deficits in the 5xFAD model. Since Aβ can inhibit long-term potentiation[72] and decreasing Aβ levels by immunization or pharmacological treatments can ameliorate cognitive deficits in APP transgenic mice,[73–75] it is accepted that the increase in Aβ levels underlies cognitive deficits in 5xFAD mice. Although additional studies are needed to determine the therapeutic window of PLGA-mediated cognitive improvement and its relationship to Aβ, these results provide compelling evidence to investigate further the potential of native PLGA in the treatment of AD pathology.

Concomitant with the attenuation of cognitive deficits, PLGA treatment markedly reduced the area, size, and number of Aβ deposits as well as ThS-positive plaques in the cortex and hippocampus of 5xFAD mice compared to the CSF-treatment group. This reduction could be due to decreased formation of new amyloid deposits and/or clearance of existing deposits because native PLGA can inhibit spontaneous Aβ aggregation and also trigger the disassembly of pre-aggregated Aβ peptides.[29,31] Since the levels of $A\beta_{1\text{-}40}$ and $A\beta_{1\text{-}42}$, as well as APP holoprotein, α-CTF, β-CTF, sAPPα, and sAPPβ, are simultaneously decreased in the cortex and hippocampus of 5xFAD mice upon treatment with PLGA, it is likely that a decrease in Aβ production partially contributes to decreased plaque load. This is consistent with our findings that the levels/activity of amyloidogenic processing enzyme BACE1 are diminished in PLGA-treated 5xFAD mice.

Transcriptomic profiling through RNAseq analysis of over 16,000 protein-coding genes across all brain samples provided comprehensive, unbiased molecular insights into the effects of PLGA administration in WT and 5xFAD mice. PCA showed that genotype and PLGA treatment explained 20% and 10% of the global transcriptomic variances, respectively. The 601 transcripts unique to PLGA-treated 5xFAD mice highlight their association with responses to external stimuli and immune effector processes. Importantly, no DEGs were found to be shared between 5xFAD PLGA versus CSF and WT PLGA versus CSF groups, suggesting that PLGA's effects are pathology-dependent.

Earlier studies reported that Aβ-induced neural network dysfunction characterized by a decrease in synapses and abnormal synaptic functions contributed to cognitive impairment and disease pathology.[76–79] Our identification of gene clusters associated with axon genesis, synapse organization, and neurotransmitter exocytosis underscore PLGA's protective role in neuronal function. Additionally, oxidative stress resulting from Aβ-induced production of toxic free radicals and/or decreased activity of antioxidant enzymes can influence synaptic loss and neurodegeneration.[64,65,80] Consistent with this notion, we observed not only increased levels of oxidative markers (i.e., carbonylated proteins and OH8dg) and decreased levels/activity of antioxidant enzyme SOD2 but also a decline in the levels of synaptophysin, PSD95, and enhanced degenerative structures in 5xFAD mice compared to WT mice. Interestingly, chronic PLGA treatment, except the post-synaptic marker PSD95, alleviated the aforementioned changes in 5xFAD mice. The identification of the cellular oxidant detoxification pathway genes in cluster 14 aligns with reduced oxidative marker levels in PLGA-treated 5xFAD mice. Elevated expression of *Gsto1*, *Gpx1*, and *Gpx3* also supports the hypothesis that PLGA treatment upregulates detoxification pathways, contributing to ROS homeostasis.

Activated astrocytes and microglia in the brain respond to Aβ accrual by triggering inflammatory responses, which lead to neuronal damage and synapse loss.[56,57] The canonical transcriptomic signatures characteristic of 5xFAD mice, such as glial activation markers (*Tyrobp*, *Gfap*, *Cd68*, *Trem2*) and enriched immune pathways, were consistent with previous 5xFAD RNA-seq data and supported by increased GFAP and CD68-positive cells in 5xFAD mice.[32,81] Additionally, we observed increased levels of astrocytic marker GFAP, microglial marker IBA1, and upregulated expression of *Gfap* and *Iba1* in the cortex and hippocampus of 5xFAD mice compared to WT controls. This is accompanied by an increased expression of CD68, a lysosomal marker of activated microglia located in the proximity of ThS-labeled neuritic plaques in 5xFAD mice. Chronic PLGA administration decreased the expression of IBA1 and GFAP in the affected regions of the 5xFAD mice. Interestingly, expression/levels of CD68 were increased in PLGA-treated 5xFAD mice compared to CSF-treated 5xFAD mice. Evidence shows that microglia gathered around neuritic plaques can phagocytize and clear Aβ via an activated lysosomal pathway.[82,83] Since CD68 represents a microglial lysosomal marker,[46,60,61] it is likely that the attenuation of Aβ plaque load in PLGA-treated 5xFAD mice may partly be mediated by enhanced microglial lysosomal activity. Our GSEA of 129 PLGA-induced DEGs in 5xFAD mice revealed that the top GO terms were related to immune response activation. A text-mining approach further illustrated the biological impact of PLGA treatment in the disease, identifying a major network of gene clusters centered on

mice and its enhancement following PLGA treatment. (K) Violin plots showing SOD2 enzyme activity in cortex and hippocampus of CSF-/PLGA-treated WT and 5xFAD mouse brains. Note decreased levels of SOD2 in 5xFAD mice compared to WT mice and its enhancement following PLGA treatment in 5xFAD mice. (L–P) Photomicrographs showing double immunolabeling with oxidative marker OH8dG (red) and OC-labeled Aβ plaques (green) in cortex of CSF-/PLGA-treated WT and 5xFAD mouse brains. As expected, oxidative marker OH8dG is evident in the 5xFAD but sparsely observed in WT mouse brain tissues. Note decrease in OH8dG-labeled neurons in PLGA-treated 5xFAD mice compared to CSF-treated 5xFAD mice. Violin plots: (B–D) One-way ANOVA with Tukey's post hoc multiple-comparisons test ($n = 4–5$ animals/group with two or three technical replicates); (J and K) Three-way ANOVA with Tukey's post hoc multiple-comparisons test ($n = 3–5$ animals/group with two or three technical replicates). $p < 0.05$ considered significant. $^{*}p < 0.05$, $^{**}p < 0.01$, $^{***}p < 0.001$. Aβ, amyloid beta; CSF, cerebrospinal fluid; PLGA, poly(D,L-lactic-co-glycolic acid); ROS, reactive oxygen species; WT, wild type.

immune response and antigen presentation themes. This may reflect a direct immune response triggered by PLGA, potentially enhancing plaque clearance, aligning with an increased CD68 levels and presence of an increased number of CD68-positive microglia in PLGA-treated 5xFAD mice.

We compared our co-expression modules with AD-related clusters generated by large-scale WGCNA analysis to identify human disease-specific modules. One interesting finding was that the blue module in our study was similar to the AD-associated immune system cluster.[55] The GSEA on the blue module confirmed the outcomes of the text-mining method. The PLGA-induced activation of *Tyrobp*, one potential phagocytosis signaling hub, could be the transcriptome evidence for elevated Aβ plaque clearance after PLGA treatment.[62] IRF8 shapes the microglia transcriptional landscape, by modulating a lysosome gene set.[63] The PLGA-induced phagocytosis, characterized by enhanced CD68 immunoreactivity, may result from the upregulated transcription factor coding gene *Irf8*. The disparate results from IBA1 and CD68 immunostaining indicate complex context-dependent microglia status subtype regulation by PLGA treatment, which underscores the need for future single-cell and spatial transcriptomic approaches to elucidate PLGA-induced responses in microglial subtypes. Nevertheless, the bulk RNA-seq analysis revealed that PLGA administration exerted its effects in 5xFAD mice through three primary mechanisms: (i) activation of microglial subtypes, (ii) maintenance of ROS balance via upregulation of detoxification pathways, and (iii) neuroprotection, characterized by improvements in the axon, synapse, neurotransmitter, and transporter functions.

Disease-modifying effective treatments for AD have yet to be developed. The drugs that have been approved, including cholinesterase inhibitors and memantine, provide only symptomatic relief for a subset of AD patients.[84] The long-term beneficial effects of recently approved Aβ antibodies lecanemab and donanemab remain to be established.[85,86] Since Aβ peptides are produced constitutively and have physiological functions in the brain,[1] it is believed that drugs targeting Aβ at different stages of pathological progression (i.e., aggregation, disaggregation, and neurotoxicity) rather than neutralizing a subset of Aβ peptides using antibodies may be more valuable in the treatment of AD pathology.[84,85]

In earlier studies, PLGA nanoparticles functionalized with donepezil, quercetin, and curcumin were found to attenuate disease pathology in AD models compared to treatment with drugs alone or the solvent used for preparing drugs/PLGA nanoparticles.[20–24,70,71] Thus, very little is known about the therapeutic potential of native PLGA in AD-related pathology. Earlier, we reported that native PLGA could (i) inhibit spontaneous aggregation and trigger disassembly of preformed Aβ fibers, (ii) protect mouse neurons and human induced pluripotent stem cell-derived neurons against Aβ-mediated toxicity.[28–30] Recently, we demonstrated that fluorescence-labeled PLGA could recognize Aβ-containing neuritic plaques in 5xFAD mice.[43] Strengthening these results, our current study reveals that chronic ICV administration of native PLGA can not only reverse cognitive deficits but also attenuate Aβ-related pathology by modulating inflammatory and oxidative stress response pathways. The evidence that PLGA can protect cultured neurons against Aβ toxicity by reducing tau phosphorylation[29,30] and inhibit Aβ-induced tau aggregation[31] raises the possibility that PLGA can regulate both Aβ and tau pathology simultaneously. Previous research showed that native PLGA could enhance lysosomal acidification, which is compromised by the buildup of toxic proteins, resulting in improved lysosomal clearance and subsequent neuronal protection.[22,23] Considering the evidence that elevated lysosomal pH promotes Aβ accumulation due to impaired degradation, which can then trigger cell death through lysosomal enzyme leakage into the cytosol,[28,87] it is possible that native PLGA, by restoring acidification and lysosomal functional integrity, could ameliorate Aβ accumulation and protect neurons in AD. Although these results need to be validated, the current study highlights the therapeutic potential of FDA-approved native PLGA in treating AD-related pathology.

ACKNOWLEDGMENTS

This work was supported by a grant from the Canadian Institutes of Health Research (CIHR) (MOP-84480) and the Alzheimer Society of Alberta and Northwest Territories to SK and grants from the National Institute on Aging, National Institutes of Health (RF1AG077610 and RF1AG079141) to GT. KG is a recipient of Ballermann Translational Research Fellowship from the Department of Medicine and SynAD postdoctoral fellowships from the University of Alberta. DG was supported by a grant from CIHR (PJT-175090) to SS.

CONFLICT OF INTEREST STATEMENT

The authors declare no conflicts of interest. Author disclosures are available in the Supporting Information.

CONSENT STATEMENT

This study did not involve any human subjects; therefore, informed consent was not required.

REFERENCES

1. Chen XQ, Mobley WC. Alzheimer disease pathogenesis: insights from molecular and cellular biology studies of oligomeric Aβ and tau species. *Front Neurosci*. 2019;13:659.
2. Bellenguez C, Grenier-Boley B, Lambert JC. Genetics of Alzheimer's disease: where we are, and where we are going. *Curr Opin Neurobiol*. 2020;61:40-48.
3. Trejo-Lopez JA, Yachnis AT, Prokop S. Neuropathology of Alzheimer's disease. *Neurotherapeutics*. 2022;19:173-185.
4. Andrew RJ, Kellett KA, Thinakaran G, Hooper NM. A greek tragedy: the growing complexity of Alzheimer amyloid precursor protein proteolysis. *J Biol Chem*. 2016;291:19235-19244.
5. Bisceglia F, Natalello A, Serafini MM, et al. An integrated strategy to correlate aggregation state, structure and toxicity of Aß 1-42 oligomers. *Talanta*. 2018;188:17-26.
6. Vetrivel KS, Cheng H, Lin W, et al. Association of γ-secretase with lipid rafts in post-Golgi and endosome membranes. *J Biol Chem*. 2004;279:44945-44954.
7. Yu W, Kumar A, Peterhoff C, et al. Autophagic vacuoles are enriched in amyloid precursor protein-secretase activities: implications for β-amyloid peptide over-production and localization in Alzheimer's disease. *Int J Biochem Cell Biol*. 2004;36:2531-2540.

8. Wang M, Jing T, Wang X, Yao D. Beta-secretase/BACE1 promotes APP endocytosis and processing in the endosomes and on cell membrane. *Neurosci Lett*. 2018;685:63-67.
9. Liu X, Liu Y, Ji S. Secretases related to amyloid precursor protein processing. *Membranes*. 2021;11:983.
10. Lee SJ, Nam E, Lee HJ, Savelieff MG, Lim MH. Towards an understanding of amyloid-β oligomers: characterization, toxicity mechanisms, and inhibitors. *Chem Soc Rev*. 2017;46:310-323.
11. Goel P, Chakrabarti S, Goel K, Bhutani K, Chopra T, Bali S. Neuronal cell death mechanisms in Alzheimer's disease: an insight. *Front Mol Neurosci*. 2022;15:937133.
12. Peng Y, Jin H, Xue YH, et al. Current and future therapeutic strategies for Alzheimer's disease: an overview of drug development bottlenecks. *Front Aging Neurosci*. 2023;15:1206572.
13. Saunders NR, Habgood MD, Møllgård K, Dziegielewska KM. The biological significance of brain barrier mechanisms: help or hindrance in drug delivery to the central nervous system?. *F1000Res*. 2016;5:F1000.
14. Kaur I, Kumar A, Behl T, Setia D. Recent advances in nanotechnology-based drug delivery approaches for Alzheimer disease. *Curr Drug Targets*. 2021;22:1404-1423.
15. Formicola B, Cox A, Dal Magro R, Masserini M, Re F. Nanomedicine for the treatment of Alzheimer's disease. *J Biomed Nanotechnol*. 2019;15:1997-2024.
16. Liu Y, Shen Y. Applications of nanoparticles in Alzheimer's disease. *J Alzheimers Dis*. 2023;96:459-471.
17. Li J, Sabliov C. PLA/PLGA nanoparticles for delivery of drugs across the blood-brain barrier. 2013;2:241-257.
18. Wang Y, Qu W, Choi S. FDA's regulatory science program for generic PLA/PLGA-based drug products. *Am Pharm Rev*. 2016;19(4):5-9.
19. Elmowafy EM, Tiboni M, Soliman ME. Biocompatibility, biodegradation and biomedical applications of poly (lactic acid)/poly (lactic-co-glycolic acid) micro and nanoparticles. *J Pharm Investig*. 2019;49:347-380.
20. Baysal I, Ucar G, Gultekinoglu M, Ulubayram K, Yabanoglu-Ciftci S. Donepezil loaded PLGA-b-PEG nanoparticles: their ability to induce destabilization of amyloid fibrils and to cross blood brain barrier in vitro. *J Neural Transm (Vienna)*. 2017;124:33-45.
21. Fornaguera C, Feiner-Gracia N, Calderó G, García-Celma MJ, Solans C. Galantamine-loaded PLGA nanoparticles, from nano-emulsion templating, as novel advanced drug delivery systems to treat neurodegenerative diseases. *Nanoscale*. 2015;7:12076-12084.
22. Fan S, Zheng Y, Liu X, et al. Curcumin-loaded PLGA-PEG nanoparticles conjugated with B6 peptide for potential use in Alzheimer's disease. *Drug Deliv*. 2018;25:1091-1102.
23. Sun D, Li N, Zhang W, et al. Design of PLGA-functionalized quercetin nanoparticles for potential use in Alzheimer's disease. *Colloids Surf B Biointerfaces*. 2016;148:116-129.
24. Sánchez-López E, Ettcheto M, Egea MA, et al. Memantine loaded PLGA PEGylated nanoparticles for Alzheimer's disease: in vitro and in vivo characterization. *J Nanobiotechnology*. 2018;16:32.
25. Baysal I, Yabanoglu-Ciftci S, Tunc-Sarisozen Y, Ulubayram K, Ucar G. Interaction of selegiline-loaded PLGA-b-PEG nanoparticles with beta-amyloid fibrils. *J Neural Transm (Vienna)*. 2013;120:903-910.
26. Baltazar GC, Guha S, Lu W, et al. Acidic nanoparticles are trafficked to lysosomes and restore an acidic lysosomal pH and degradative function to compromised ARPE-19 cells. *PLoS One*. 2012;7:e49635.
27. Bourdenx M, Daniel J, Genin E, et al. Nanoparticles restore lysosomal acidification defects: implications for Parkinson and other lysosomal-related diseases. *Autophagy*. 2016;12:472-483.
28. Wang Y, Wu Q, Anand BG, et al. Significance of cytosolic cathepsin D in Alzheimer's disease pathology: protective cellular effects of PLGA nanoparticles against β-amyloid-toxicity. *Neuropathol Appl Neurobiol*. 2020;46:686-706.
29. Anand B, Wu Q, Nakhaei-Nejad M, et al. Significance of native PLGA nanoparticles in the treatment of Alzheimer's disease pathology. *Bioact Mater*. 2022;17:506-525.
30. Wu Q, Karthivashan G, Nakhaei-Nejad M, Anand BG, Giuliani F, Kar S. Native PLGA nanoparticles regulate APP metabolism and protect neurons against β-amyloid toxicity: potential significance in Alzheimer's disease pathology. *Int J Biol Macromol*. 2022;219:1180-1196.
31. Paul PS, Cho JY, Wu Q, et al. Unconjugated PLGA nanoparticles attenuate temperature-dependent β-amyloid aggregation and protect neurons against toxicity: implications for Alzheimer's disease pathology. *J Nanobiotechnology*. 2022;20:67.
32. Forner S, Kawauchi S, Balderrama-Gutierrez G, et al. Systematic phenotyping and characterization of the 5xFAD mouse model of Alzheimer's disease. *Sci Data*. 2021;8:270.
33. Di Pardo A, Maglione V, Alpaugh M, et al. Ganglioside GM1 induces phosphorylation of mutant huntingtin and restores normal motor behavior in Huntington disease mice. *Proc Natl Acad Sci U S A*. 2012;109:3528-3533.
34. Vaucher E, Aumont N, Pearson D, Rowe W, Poirier J, Kar S. Amyloid beta peptide levels and its effects on hippocampal acetylcholine release in aged, cognitively-impaired and -unimpaired rats. *J Chem Neuroanat*. 2001;21:323-329.
35. Gourmaud S, Thomas P, Thomasseau S, et al. Brimapitide reduced neuronal stress markers and cognitive deficits in 5XFAD transgenic mice. *J Alzheimers Dis*. 2018;63:665-674.
36. Song MS, Rauw G, Baker GB, Kar S. Memantine protects rat cortical cultured neurons against beta-amyloid-induced toxicity by attenuating tau phosphorylation. *Eur J Neurosci*. 2008;28:1989-2002.
37. Ponnusamy M, Wang S, Yuksel M, et al. Loss of forebrain BIN1 attenuates hippocampal pathology and neuroinflammation in a tauopathy model. *Brain*. 2023;146:1561-1579.
38. Schmued LC, Stowers CC, Scallet AC, Xu L. Fluoro-Jade C results in ultra high resolution and contrast labeling of degenerating neurons. *Brain Res*. 2005;1035:24-31.
39. Maulik M, Peake K, Chung J, Wang Y, Vance JE, Kar S. APP overexpression in the absence of NPC1 exacerbates metabolism of amyloidogenic proteins of Alzheimer's disease. *Hum Mol Genet*. 2015;24:7132-7150.
40. Szychowski KA, Wnuk A, Rzemieniec J, Kajta M, Leszczyńska T, Wójtowicz AK. Triclosan-evoked neurotoxicity involves NMDAR subunits with the specific role of GluN2A in caspase-3-dependent apoptosis. *Mol Neurobiol*. 2019;56:1-12.
41. Sheng X, Yang Y, Zhou J, et al. Mitochondrial transfer from aged adipose-derived stem cells does not improve the quality of aged oocytes in C57BL/6 mice. *Mol Reprod Dev*. 2019;86:516-529.
42. Dahal A, Govindarajan K, Kar S. Administration of kainic acid differentially alters astrocyte markers and transiently enhanced phospho-tau level in adult rat hippocampus. *Neuroscience*. 2023;516:27-41.
43. Govindarajan K, Kar S. Correction: detection of β-amyloid aggregates/plaques in 5xFAD mice by labelled native PLGA nanoparticles: implication in the diagnosis of Alzheimer's disease. *J Nanobiotechnology*. 2023;21:251.
44. Oakley H, Cole SL, Logan S, et al. Intraneuronal beta-amyloid aggregates, neurodegeneration, and neuron loss in transgenic mice with five familial Alzheimer's disease mutations: potential factors in amyloid plaque formation. *J Neurosci*. 2006;26:10129-10140.
45. Jawhar S, Trawicka A, Jenneckens C, Bayer TA, Wirths O. Motor deficits, neuron loss, and reduced anxiety coinciding with axonal

degeneration and intraneuronal Aβ aggregation in the 5XFAD mouse model of Alzheimer's disease. *Neurobiol Aging*. 2012;33:196.e29-40.
46. Jo KW, Lee D, Cha DG, et al. Gossypetin ameliorates 5xFAD spatial learning and memory through enhanced phagocytosis against Aβ. *Alzheimers Res Ther*. 2022;14:158.
47. Pádua MS, Guil-Guerrero JL, Lopes PA. Behaviour hallmarks in Alzheimer's disease 5xFAD mouse model. *Int J Mol Sci*. 2024;25(12):6766.
48. Maarouf CL, Kokjohn TA, Whiteside CM, et al. Molecular differences and similarities between Alzheimer's disease and the 5XFAD transgenic mouse model of amyloidosis. *Biochem Insights*.. 2013;6:1-10.
49. Devi L, Ohno M. Effects of BACE1 haploinsufficiency on APP processing and Aβ concentrations in male and female 5XFAD Alzheimer mice at different disease stages. *Neuroscience*. 2015;307:128-137.
50. Gutiérrez IL, González-Prieto M, García-Bueno B, Caso JR, Leza JC, Madrigal JLM. Alternative method to detect neuronal degeneration and amyloid β accumulation in free-floating brain sections with fluoro-jade. *ASN Neuro*. 2018;10:1759091418784357.
51. Henningfield CM, Soni N, Lee RW, Sharma R, Cleland JL, Green KN. Selective targeting and modulation of plaque associated microglia via systemic hydroxyl dendrimer administration in an Alzheimer's disease mouse model. *Alzheimers Res Ther*. 2024;16:101.
52. Landel V, Baranger K, Virard I, et al. Temporal gene profiling of the 5XFAD transgenic mouse model highlights the importance of microglial activation in Alzheimer's disease. *Mol Neurodegener*. 2014;9:33.
53. Boza-Serrano A, Yang Y, Paulus A, Deierborg T. Innate immune alterations are elicited in microglial cells before plaque deposition in the Alzheimer's disease mouse model 5xFAD. *Sci Rep*. 2018;8:1550.
54. Manji Z, Rojas A, Wang W, Dingledine R, Varvel NH, Ganesh T. 5xFAD mice display sex-dependent inflammatory gene induction during the prodromal stage of Alzheimer's disease. *J Alzheimers Dis*. 2019;70:1259-1274.
55. Wan Y-W, Al-Ouran R, Mangleburg CG, et al. Meta-analysis of the Alzheimer's disease human brain transcriptome and functional dissection in mouse models. *Cell Rep*. 2020;32:107908.
56. Kaur D, Sharma V, Deshmukh R. Activation of microglia and astrocytes: a roadway to neuroinflammation and Alzheimer's disease. *Inflammopharmacology*. 2019;27:663-677.
57. Liu K, Aierken A, Liu M, et al. The decreased astrocyte-microglia interaction reflects the early characteristics of Alzheimer's disease. *iScience*. 2024;27:109281.
58. Companys-Alemany J, Turcu AL, Vázquez S, Pallàs M, Griñán-Ferré C. Glial cell reactivity and oxidative stress prevention in Alzheimer's disease mice model by an optimized NMDA receptor antagonist. *Sci Rep*. 2022;12:17908.
59. Lee CYD, Daggett A, Gu X, et al. Elevated TREM2 gene dosage reprograms microglia responsivity and ameliorates pathological phenotypes in Alzheimer's disease models. *Neuron*. 2018;97:1032-1048.e5.
60. Pan RY, Ma J, Kong XX, et al. Sodium rutin ameliorates Alzheimer's disease-like pathology by enhancing microglial amyloid-β clearance. *Sci Adv*. 2019;5:eaau6328.
61. Choi C, Kim H, Oh J, et al. DSCR1 deficiency ameliorates the Aβ pathology of Alzheimer's disease by enhancing microglial activity. *Life Sci Alliance*. 2023;6(2):e202201556.
62. Haure-Mirande JV, Audrain M, Ehrlich ME, Gandy S. Microglial TYROBP/DAP12 in Alzheimer's disease: transduction of physiological and pathological signals across TREM2. *Mol Neurodegener*. 2022;17:55.
63. Saeki K, Pan R, Lee E, Kurotaki D, Ozato K. IRF8 defines the epigenetic landscape in postnatal microglia, thereby directing their transcriptome programs. *Nat Immunol*. 2024;25:1928-1942.
64. Murakami K, Murata N, Noda Y, et al. SOD1 (copper/zinc superoxide dismutase) deficiency drives amyloid β protein oligomerization and memory loss in mouse model of Alzheimer disease. *J Biol Chem*. 2011;286:44557-44568.
65. Liu Z, Kumar M, Kabra A. Cucurbitacin B exerts neuroprotection in a murine Alzheimer's disease model by modulating oxidative stress, inflammation, and neurotransmitter levels. *Front Biosci (Landmark Ed)*. 2022;27:71.
66. Smith DG, Cappai R, Barnham KJ. The redox chemistry of the Alzheimer's disease amyloid β peptide. *Biochim Biophys Acta*. 2007;1768:1976-1990.
67. Sonnen JA, Breitner JC, Lovell MA, Markesbery WR, Quinn JF, Montine TJ. Free radical-mediated damage to brain in Alzheimer's disease and its transgenic mouse models. *Free Radic Biol Med*. 2008;45:219-230.
68. Üremiş N, Üremiş MM. Oxidative/nitrosative stress, apoptosis, and redox signaling: key players in neurodegenerative diseases. *J Biochem Mol Toxicol*. 2025;39:e70133.
69. Cunha A, Gaubert A, Latxague L, Dehay B. PLGA-Based nanoparticles for neuroprotective drug delivery in neurodegenerative diseases. *Pharmaceutics*. 2021;13:1042.
70. Aalinkeel R, Kutscher HL, Singh A, et al. Neuroprotective effects of a biodegradable poly(lactic-co-glycolic acid)-ginsenoside Rg3 nanoformulation: a potential nanotherapy for Alzheimer's disease? *J Drug Target*. 2018;26:182-193.
71. Jeon SG, Cha MY, Kim JI, et al. Vitamin D-binding protein-loaded PLGA nanoparticles suppress Alzheimer's disease-related pathology in 5XFAD mice. *Nanomedicine*. 2019;17:297-307.
72. Chen QS, Kagan BL, Hirakura Y, Xie CW. Impairment of hippocampal long-term potentiation by Alzheimer amyloid beta-peptides. *J Neurosci Res*. 2000;60:65-72.
73. Schenk D, Barbour R, Dunn W, et al. Immunization with amyloid-beta attenuates Alzheimer-disease-like pathology in the PDAPP mouse. *Nature*. 1999;400:173-177.
74. Bartus RT, Dean RL 3rd. Pharmaceutical treatment for cognitive deficits in Alzheimer's disease and other neurodegenerative conditions: exploring new territory using traditional tools and established maps. *Psychopharmacology (Berl)*. 2009;202:15-36.
75. Vogt AS, Jennings GT, Mohsen MO, Vogel M, Bachmann MF. Alzheimer's disease: a brief history of immunotherapies targeting amyloid β. *Int J Mol Sci*. 2023;24:3895.
76. Dong H, Martin MV, Chambers S, Csernansky JG. Spatial relationship between synapse loss and beta-amyloid deposition in Tg2576 mice. *J Comp Neurol*. 2007;500:311-321.
77. Peña-Ortega F. Amyloid beta-protein and neural network dysfunction. *J Neurodegener Dis*. 2013;2013:657470.
78. Kaufman AC, Salazar SV, Haas LT, et al. Fyn inhibition rescues established memory and synapse loss in Alzheimer mice. *Ann Neurol*. 2015;77:953-971.
79. Mabrouk R, Miettinen PO, Tanila H. Most dystrophic neurites in the common 5xFAD Alzheimer mouse model originate from axon terminals. *Neurobiol Dis*. 2023;182:106150.
80. Bello-Medina PC, González-Franco DA, Vargas-Rodríguez I, Díaz-Cintra S. Oxidative stress, the immune response, synaptic plasticity, and cognition in transgenic models of Alzheimer disease. *Neurologia (Engl Ed)*. 2022;37:682-690.
81. Bundy JL, Vied C, Badger C, Nowakowski RS. Sex-biased hippocampal pathology in the 5XFAD mouse model of Alzheimer's disease: a multi-omic analysis. *J Comp Neurol*. 2019;527:462-475.
82. Shi Q, Chang C, Saliba A, Bhat MA. Microglial mTOR activation upregulates trem2 and enhances β-amyloid plaque clearance in the 5XFAD Alzheimer's disease model. *J Neurosci*. 2022;42:5294-5313.

83. Ni J, Xie Z, Quan Z, Meng J, Qing H. How brain 'cleaners' fail: mechanisms and therapeutic value of microglial phagocytosis in Alzheimer's disease. *Glia*. 2024;72:227-244.
84. Jeremic D, Jiménez-Díaz L, Navarro-López JD. Past, present and future of therapeutic strategies against amyloid-β peptides in Alzheimer's disease: a systematic review. *Ageing Res Rev*. 2021;72:101496.
85. Avgerinos KI, Ferrucci L, Kapogiannis D. Effects of monoclonal antibodies against amyloid-β on clinical and biomarker outcomes and adverse event risks: a systematic review and meta-analysis of phase III RCTs in Alzheimer's disease. *Ageing Res Rev*. 2021;68:101339.
86. Larkin HD. Lecanemab gains FDA approval for early Alzheimer disease. *JAMA*. 2023;329:363.
87. Nixon RA. Autophagy–lysosomal-associated neuronal death in neurodegenerative disease. *Acta Neuropathologica*. 2024;148:42.

SUPPORTING INFORMATION

Additional supporting information can be found online in the Supporting Information section at the end of this article.

How to cite this article: Karthivashan G, Wang S, Wu Q, et al. Native PLGA nanoparticles attenuate disease pathology via multiple pathways in 5xFAD Alzheimer's model. *Alzheimer's Dement*. 2026;22:e71348. https://doi.org/10.1002/alz.71348